UNIVERSITY
OF
QUEENSLAND

Department of Civil Engineering

RESEARCH REPORT SERIES

Blockage and Aspect Ratio Effects on Flow Past a Circular Cylinder for $10^4 < R < 10^5$

WEST and C.J. APELT

search Report No. CE29
October, 1981

CIVIL ENGINEERING RESEARCH REPORTS

This report is one of a continuing series of Research Reports published by the Department of Civil Engineering at the University of Queensland. This Department also publishes a continuing series of Bulletins. Lists of recently published titles in both of these series are provided inside the back cover of this report. Requests for copies of any of these documents should be addressed to the Departmental Secretary.

The interpretations and opinions expressed herein are solely those of the author(s). Considerable care has been taken to ensure the accuracy of the material presented. Nevertheless, responsibility for the use of this material rests with the user.

Department of Civil Engineering,
University of Queensland,
St Lucia, Q 4067, Australia,
[Tel:(07) 377-3342, Telex:UNIVQLD AA40315]

BLOCKAGE AND ASPECT RATIO EFFECTS ON FLOW PAST A CIRCULAR CYLINDER FOR $10^4 < R < 10^5$

by

G.S. West, BSc *Lond.*, ME, MICE, MIMechE
Senior Lecturer in Civil Engineering

and

C.J. Apelt, DPhil *Oxon*, BE, FIE Aust
Professor of Civil Engineering

RESEARCH REPORT NO. CE 29
Department of Civil Engineering
University of Queensland
October, 1981

Synopsis

A series of experiments has produced comparable results in which the relatively small changes in the flow past a circular cylinder associated with varying blockage ratios can be clearly distinguished. The experiments cover a range of blockage from 2 to 16% and of aspect ratios from 4 to 10. End plates were fitted to the cylinders.

For blockage ratios less than 6%, it is shown that the effects of blockage on pressure distribution and the drag coefficient are small and that the Strouhal number is unaffected by blockage. For blockage ratios in the range 6-16% the effects are complex. The pressure distribution is of a different form and the Strouhal number changes. However, conflicting influences result in a blocked drag coefficient which is not very different from that at no blockage.

CONTENTS

1. INTRODUCTION

Experimental studies of flow past a circular cylinder have provided large amounts of data concerning pressure distribution, drag coefficient and vortex shedding and valuable reviews have been compiled by Morkovin (1964) and Lienhard (1966). Blockage correction procedures have been reviewed by Modi and El-Sherbiny (1971) and Farell *et al.* (1977) in the light of their own and other experiments but, in spite of the considerable volume of published data, lack of consistency in controlling or reporting secondary parameters, particularly aspect ratio and background turbulence, in different studies has made comparisons difficult. To rectify this a programme of essentially simple experiments was embarked upon to acquire accurate, comparable data. The emphasis throughout was on accuracy of measurement and control of these secondary parameters in order to avoid masking the small changes associated with blockage.

The data, obtained principally from surface pressure measurements on the cylinder but also relating to wake frequencies and tunnel-wall pressures, are presented, generally in graphical form.

2. EQUIPMENT

The wind tunnel is shown diagrammatically in Figure 1(a) and was used throughout. It is an open circuit tunnel discharging to atmosphere outside the laboratory and with a parallel-sided, closed-working section 300 mm square with 60 mm corner fillets. The intake, screens and settling chamber result in low turbulence (less than 0.15%) and a very uniform velocity distribution, the departures from uniformity being so small that they are less than the accuracy of measurement. All measurements, unless otherwise stated, were taken with the models mounted horizontally on the centre-line one quarter way along the working section. The axial flow fan was driven by a variable-speed motor and flow conditions were monitored constantly by the pressure drop across the upstream contraction.

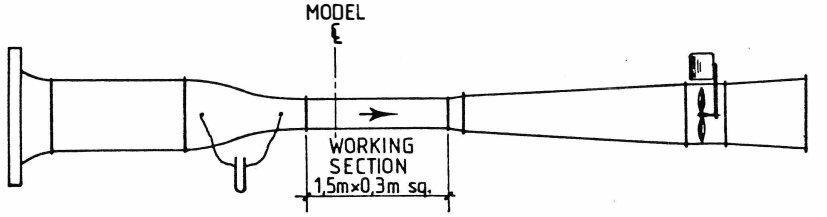

(a)

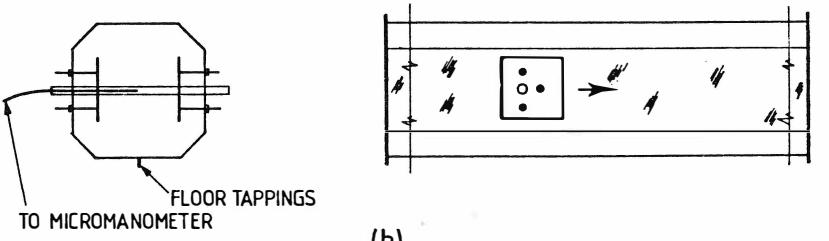

(b)

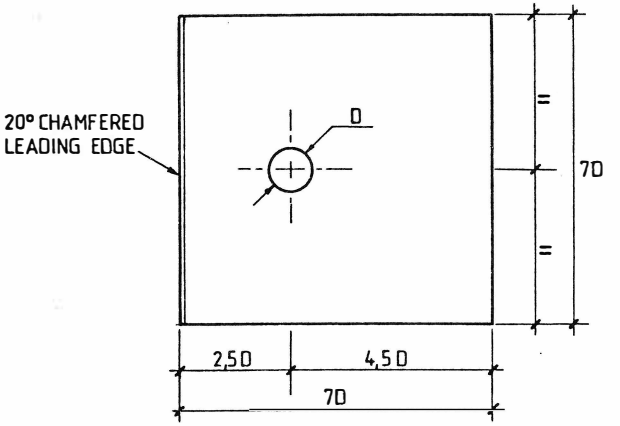

(c)

FIGURE 1 : (a) The wind tunnel, (b) Model mounting arrangement, (c) Geometry of end plates

A single row of pressure tappings was provided along the centre-line of the tunnel floor.

The models were polished brass cylinders, each having a single small (0.5 mm diameter) pressure tapping near its mid-length. They were mounted in a protractor at the tunnel wall, calibrated in 1^{o} divisions and capable of rotation in 10^{o} steps. Seven models were used with diameters varying from 3.2 mm (2% blockage) to 41 mm (16% blockage). The aspect ratio of the cylinders was controlled by end plates, as shown in Figure 1(b). Four aspect rations, 4, 6, 8 and 10, were used.

Pressure measurement on the models were made with projection micromanometers (Betz-type) by T.E.M. of Crawley, England, and these were also used to monitor the wind tunnel velocity. Tunnel-floor pressures were read on a standard multi-tube inclined alcohol manometer bank. Vortex-shedding frequencies and wake characteristics were measured with DISA M10 constant-temperature hot-wire anemometer equipment and ancillary devices such as a function generator and Tektronix 5000 series oscilloscope.

3. EXPERIMENTAL TECHNIQUE

The tunnel was operated in conventional fashion by calibrating the contraction differential pressure against a Pitot-static tube at the model position with the tunnel empty and using this calibration to give test conditions with the model installed. The tunnel static pressure was calculated from the stagnation-point pressure on the upstream side of the cylinder and the approach velocity. In calculating the air density, allowance was made for variations in barometric conditions and for the variable pressure loss between tunnel entry and working section.

Model surface pressure measurements were very time-consuming owing to the slow response of the water-filled manometers but great accuracy was possible (0.2 mm of water) and all tests were performed at least twice to check their

repeatability. Pressure measurements were always repeatable to within 0.2 mm of water. The micromanometers are not temperature compensated and temperature variations in the laboratory can be considerable so that it was necessary to adjust the zero settings of the micromanometers frequently when extreme accuracy was required. The model orientation was determined by first establishing the stagnation point from the symmetry of the flow fields and thereafter by operating in $\pm$ 10^{o} steps.

Smooth aluminium end plates were used to minimize interaction between the tunnel-wall boundary layer and the wake of the model, previous work having shown a substantial rise in wake pressure if these were omitted. The proportions of the plates are shown in Figure 1(c) and are those resulting from the optimization experiments by Stansby (1974). The model passed through a very neat hole in each end-plate with effectively no clearance and the centre section of the tunnel was free of all obstructions. The end-plates were all geometrically similar and care was taken to ensure that they were maintained in the correct orientation, parallel to the flow, particularly at small aspect-ratio settings.

The blockage figures quoted have been calculated from the gross frontal area of the model assembly and therefore include a small contribution from the end plates and mounting tubes. It is arguable that the mounting tubes should not be included in the blockage but their contribution is small and, either way, the displacement of any plotted point would be very small.

The vortex frequencies were found from Lissajous figures on the oscilloscope, the hot-wire signal being run against a function generator. The hot-wire probe was located just outside the near wake, approximately two cylinder diameters downstream and one diameter above the model centre to give the cleanest trace.

Wake profiles were plotted on a comparative basis using the arbitrary definition that "The wake boundary is where the local velocity is the same as it was in the empty tunnel, for the same approach conditions".

During the experimental programme the following secondary matters were considered:

(a) *Spanwise pressure variation.* A cylinder with pressure tappings along a generator demonstrated that there was no measurable spanwise pressure variation between end-plates. Initial measurements with this model appeared to show some variation but this was traced to imperfections in manufacture. Very great care is necessary in the location and drilling of the pressure tappings.

(b) *Tunnel-wall boundary-layer interference.* It was thought possible that, when the blockage was substantial, there might be interaction between the tunnel-wall boundary layer and the cylinder despite the use of end plates. One model with blockage of 9% was therefore tested over the full range of Reynolds number and aspect ratio while located near the downstream end of the wind-tunnel working section, where the wall boundary layer was much thicker. This change in the tunnel-wall boundary layers had no effect on the results.

(c) *Very small models.* The pressure tappings and surface finish could not be correctly scaled nor could standard end plate mountings be used. Consequently there is rather less accuracy with the smallest two models; the trend of the results is reliable but absolute values are less so. This can be seen in Figures 2 - 5.

(d) *Tunnel pressure gradient.* In standard configuration the working section is parallel-sided so that boundary-layer growth induces a small negative pressure gradient. One model (9% blockage) was tested at an intermediate Reynolds number (6×10^4) with the wind-tunnel wall panels modified to give zero pressure gradient in the empty working section. No appreciable change from the results obtained under standard conditions could be detected.

(e) *High-Reynolds-number flows.* The 12.5 blockage model at maximum tunnel speed 'tripped' into the transition

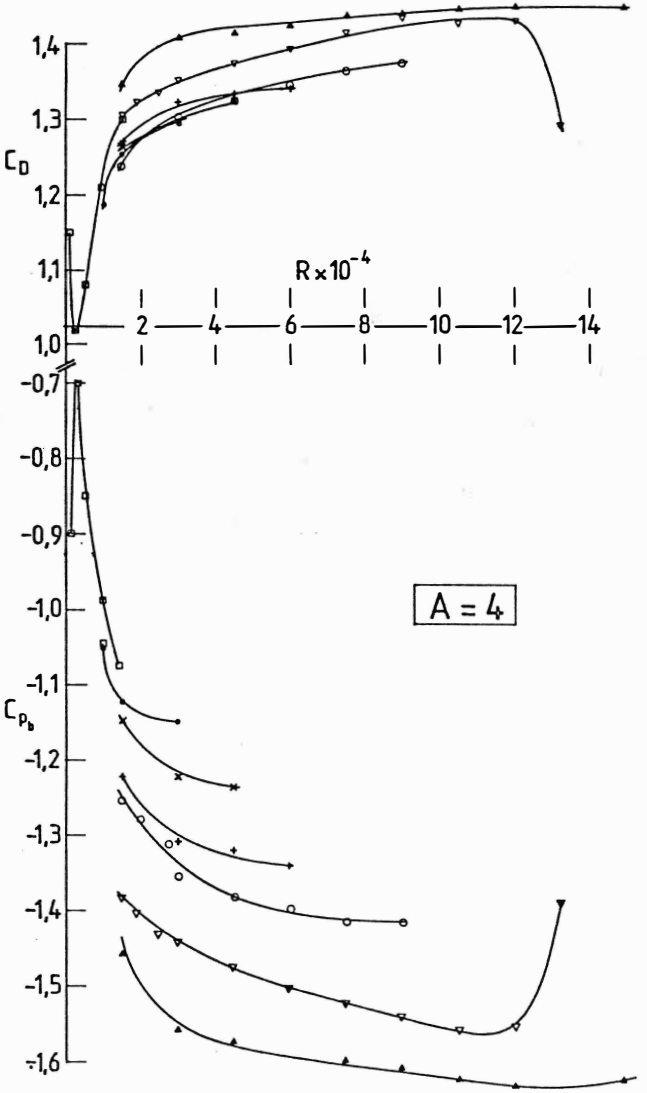

FIGURE 2 : Variation of drag coefficient and base-pressure coefficient with Reynolds number at aspect ratio 4. Blockage ratio: ▲, 16%; ▽, 12.5%; o, 9.3%; +, 6%; x, 3.5%; ●, 2.4%; □, 1.2%.

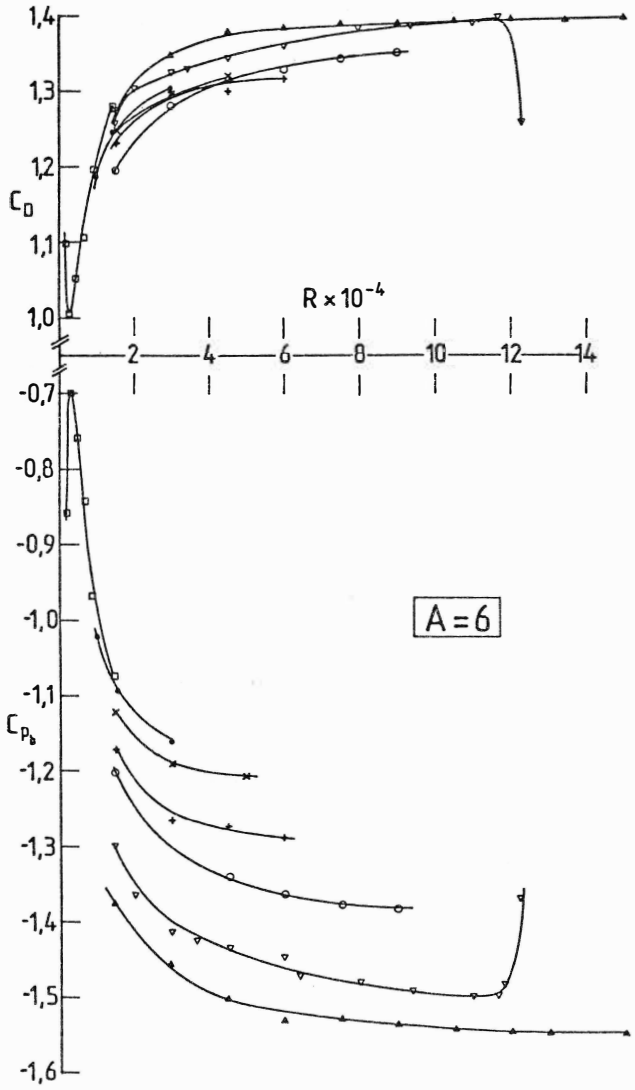

FIGURE 3 : Variation of drag coefficient and base-pressure coefficient with Reynolds number at aspect ratio 6. Blockage ratio: ▲, 15.2%; ▽, 12.3%; o, 9%; +, 5.8%; x, 3.5%; ●, 2.4%; □, 1.2%.

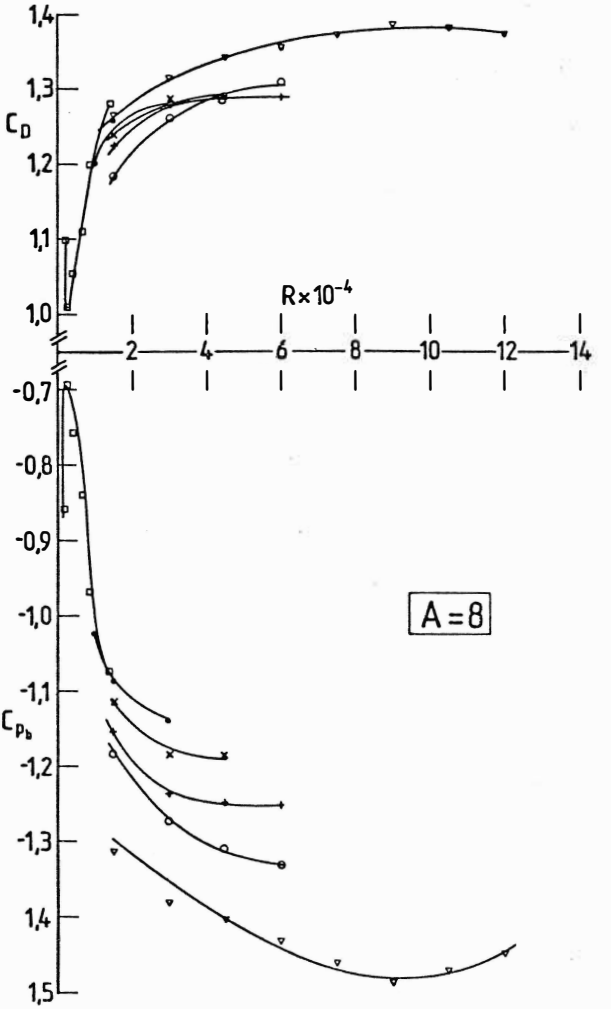

FIGURE 4 : Variation of drag coefficient and base-pressure coefficient with Reynolds number at aspect ratio 8. Blockage ratio: ▽, 12%; o, 8.8%; +, 5.65%; x, 3.5%; ●, 2.4%; □, 1.2%.

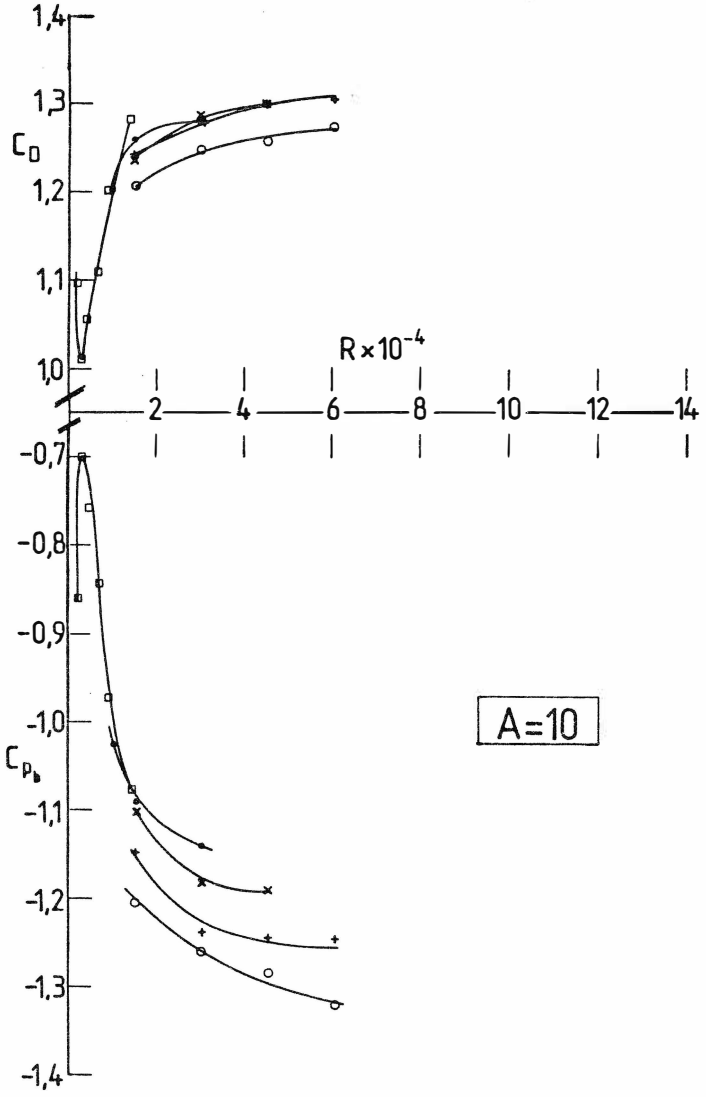

FIGURE 5 : Variation of drag coefficient and base-pressure coefficient with Reynolds number at aspect ratio 10. Blockage ratio: o, 8.6%; +, 5.5%; x, 3.5%; ●, 2.4%; □, 1.2%.

condition at aspect ratios of 4 and 6 but not at 8. Further, the 16% blockage model, which achieved a rather higher Reynolds number for A = 4, 6, would not go into transition at all.

(f) *Low-Reynolds-number flows.* The results obtained with the smallest cylinder display a marked increase in base pressure coefficient as the Reynolds number is decreased from 10 000 until a maximum is reached at a Reynolds number of 3 000. As the Reynolds number is reduced further the base pressure coefficient decreases again. Over the same range of Reynolds number there is a corresponding reverse variation of drag coefficient with a minimum occurring at Reynolds number of 3 000. Studies by Gerrard (1965) and by Roshko and Fiszdon (1969) have shown that, as the Reynolds number varies between 10^3 and 10^4, the flow undergoes quite complex changes. It would be of interest to explore the effects of blockage in this range but this was not possible with the facilities available.

4. RESULTS

The notation which is used in the figures and discussion is shown in Appendix C.

Figures 2 - 5 show all the integrated results of the surface pressure measurements for the four aspect ratios tested. In each case the Reynolds-number range was limited at the lower end by the minimum pressure difference that could be measured accurately and at the upper end by the power limit at the fan. Each drag coefficient was calculated from a plotted pressure distribution curve and the base pressures quoted were at 180° from the stagnation point. If the base pressure is defined as the mean value over the region of θ = 135 to 180°, curves of similar shape are obtained.

The results may be plotted against blockage or aspect ratio instead of Reynods number and examples of these presentations are given in Figures 6 and 7. Any others that

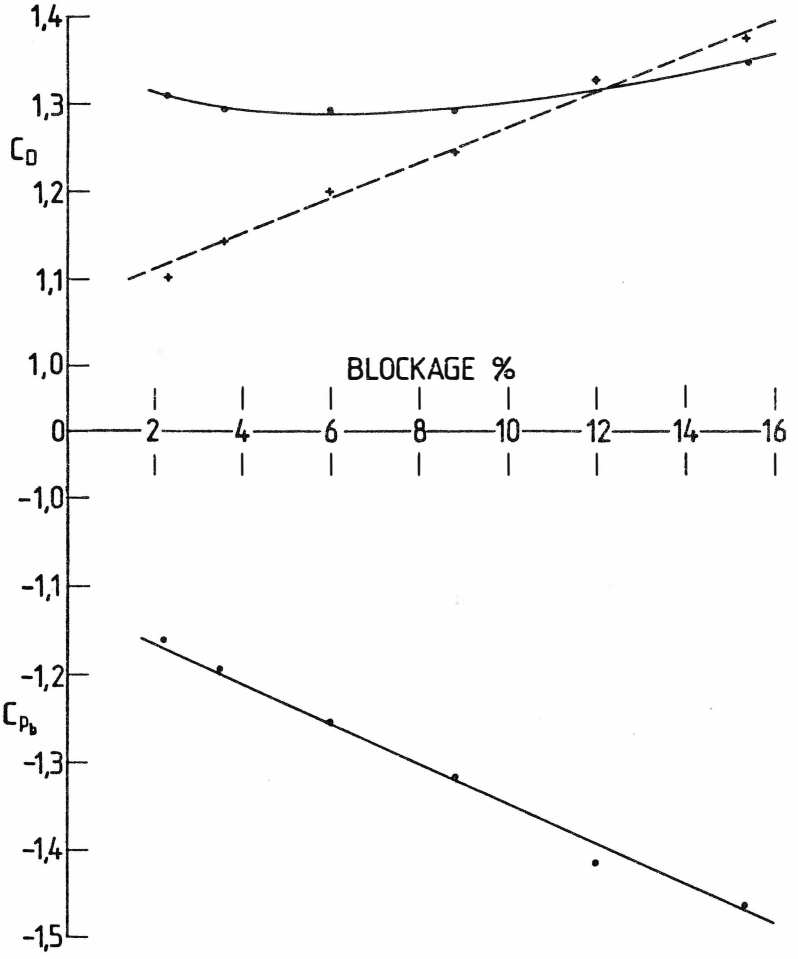

FIGURE 6 : Variation of drag coefficient and base-pressure coefficient with blockage at R = 3 x 10^4, A = 6; ●, $C_{D\ total}$; +, $C_{D(90-180)}$.

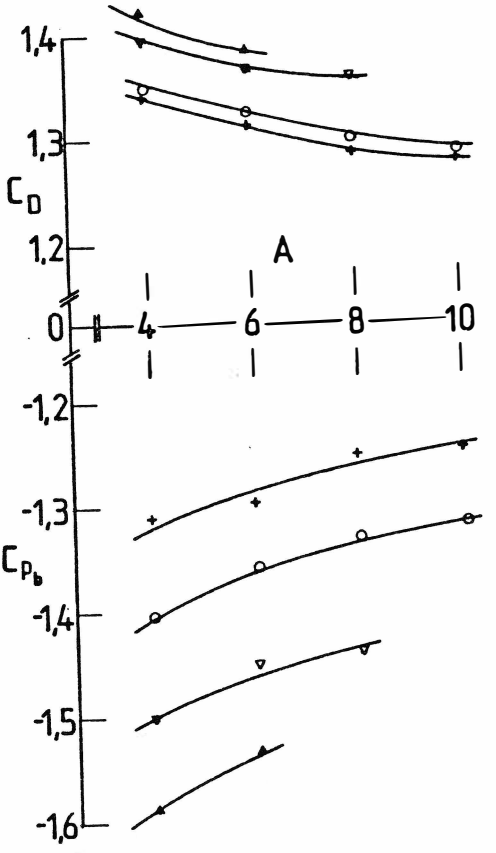

FIGURE 7 : Variation of drag coefficient and base-pressure coefficient with aspect ratio at R = 6 x 10^4. Blockage ratio: ▲, 16%; ▽, 12.5%; o, 9%; +, 6%.

may be required can be transposed from Figures 2 - 5 or plotted from the tabulated results in Appendix B. Figure 6 also shows (the dashed line) the contribution of the rear half of the cylinder only to the drag coefficient, denoted by $C_{D(90-180)}$.

The pressure distributions that give rise to the above results are shown in Figures 8.1 - 8.26 at Reynolds number increments of 1.5×10^4 and aspect rations 4, 6, 8, 10. The only singularity was the isolated case in the critical regime at high Reynolds number and blockage but this, though interesting, is not relevant here.

Figure 9 summarizes the behaviour of the floor pressure coefficients with one case of low and one of high blockage. If the blockage is 6% or less no variation with blockage can be detected; from 6 to 16% the variation is progressive. In all cases there is gradual variation with Reynolds number within the bandwidth shown.

Figures 10 and 11 show the wake frequency characteristics in two alternative forms, Figure 11 being derived from Figure 10. Again the results for low blockage flows lie so close together that a single line has been drawn through them in Figure 10, corresponding to the horizontal segments of the curves in Figure 11.

Beyond the range of parameters investigated systematically, results were obtained for two cases with much larger aspect ratios, again with standard end plates, and these are shown in Figures 12 and 13. It appears from these results that variations with aspect ratio continue further than is generally realized.

Figure 15 shows the wake profiles at one particular Reynolds number, 2.75×10^4. This was the only condition tested and showed the expected wake width reduction with increase of blockage. It is intended to obtain further data but the large time commitment involved precluded further work at this stage.

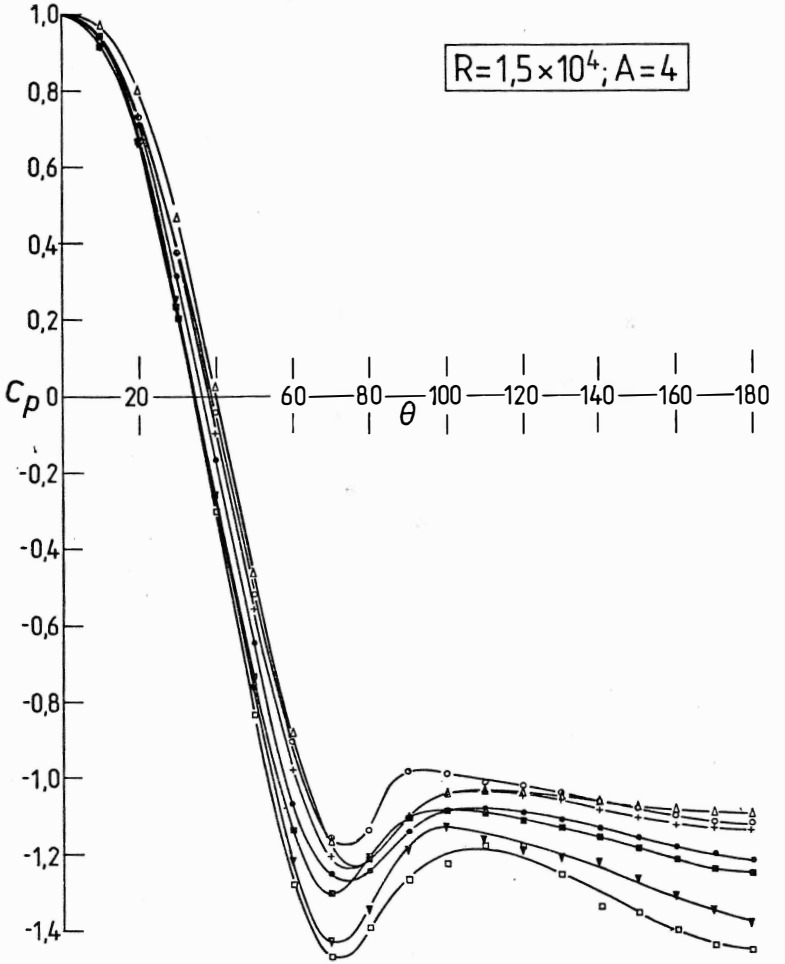

FIGURE 8.1 : Pressure distribution around cylinder. Blockage ratio: △, 1.2%; o, 2.4%; +, 3.5%; ●, 5.8%; ■, 9%; ▼, 12.3%; □, 15.2%.

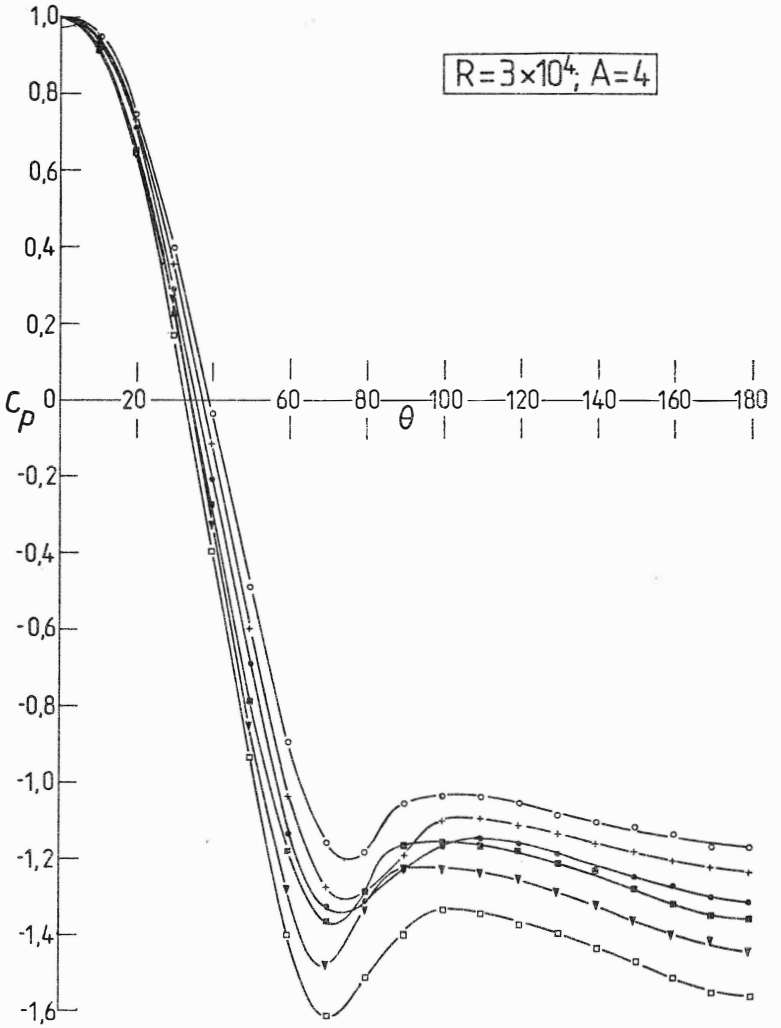

FIGURE 8.2 : Pressure distribution around cylinder. Blockage ratio: △, 1.2%; ○, 2.4%; +, 3.5%; ●, 5.8%; ■, 9%; ▼, 12.3%; □, 15.2%.

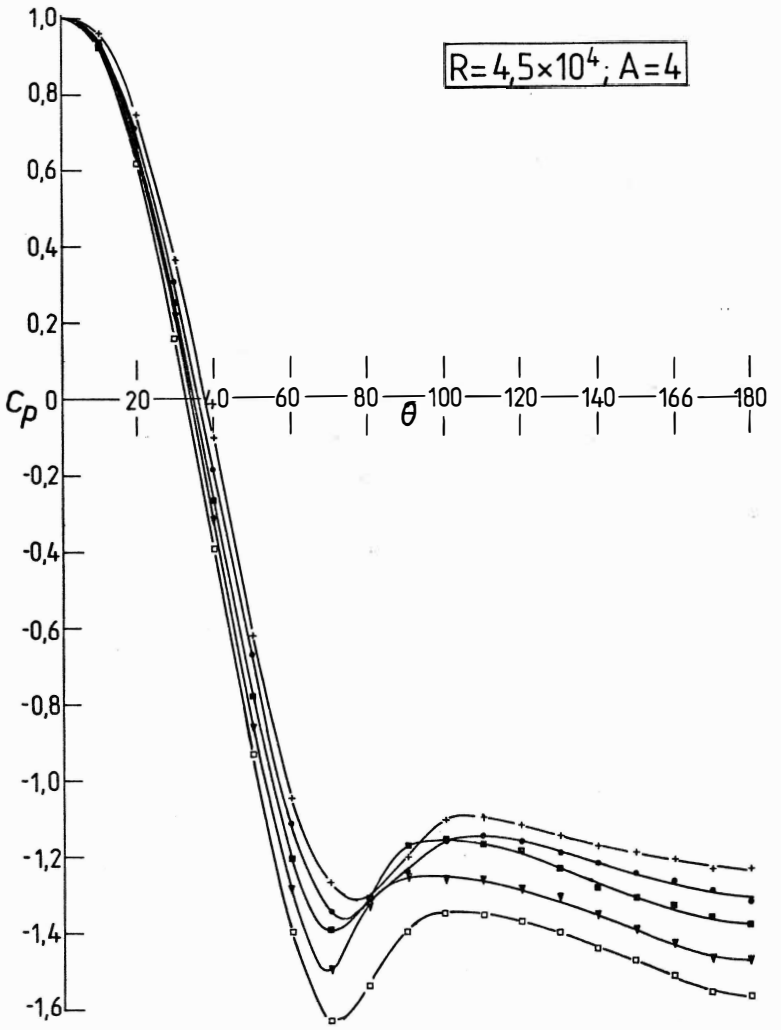

FIGURE 8.3 : Pressure distribution around cylinder. Blockage ratio: Δ, 1.2%; o, 2.4%; +, 3.5%; ●, 5.8%; ■, 9%; ▼, 12.3%; □, 15.2%.

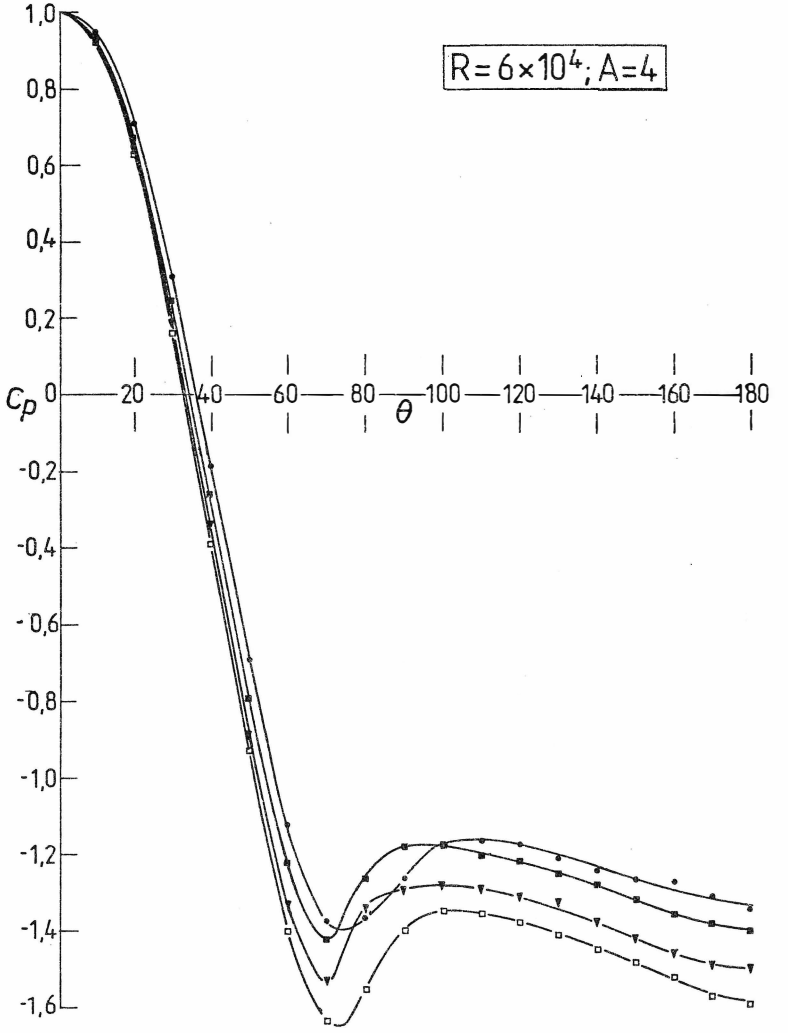

FIGURE 8.4 : Pressure distribution around cylinder. Blockage ratio: Δ, 1.2%; o, 2.4%; +, 3.5%; ●, 5.8%; ■, 9%; ▼, 12.3%; □, 15.2%.

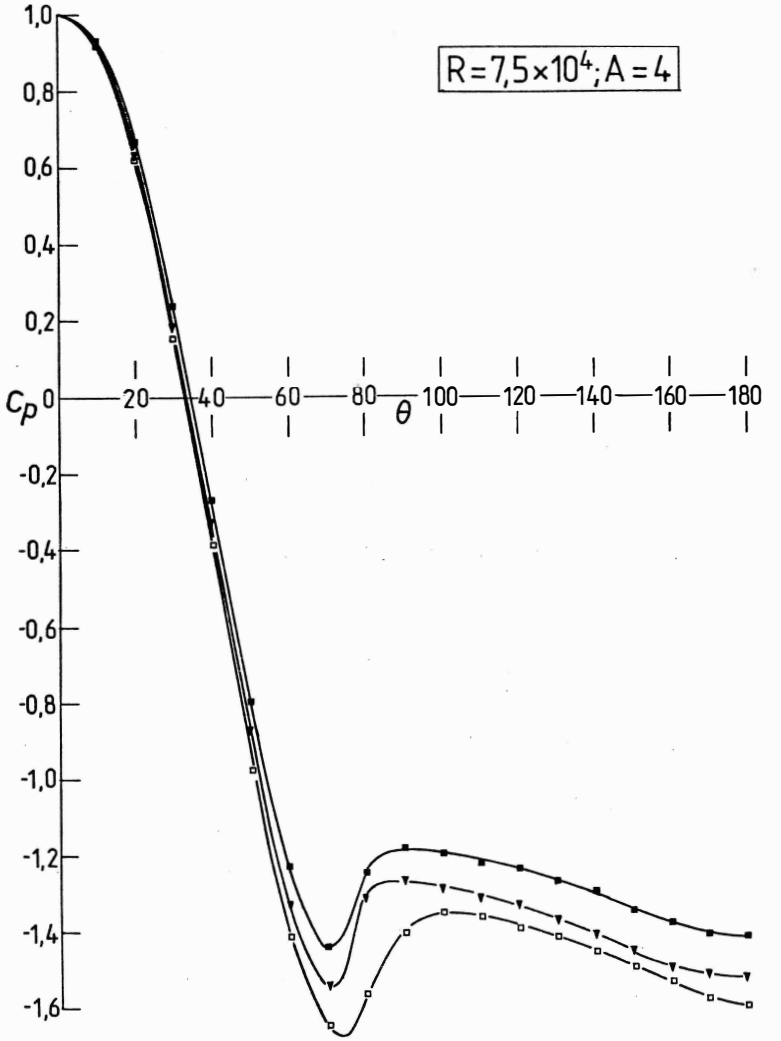

FIGURE 8.5 : Pressure distribution around cylinder. Blockage ratio: △, 1.2%; o, 2.4%; +, 3.5%; ●, 5.8%; ■, 9%; ▼, 12.3%; [], 15.2%.

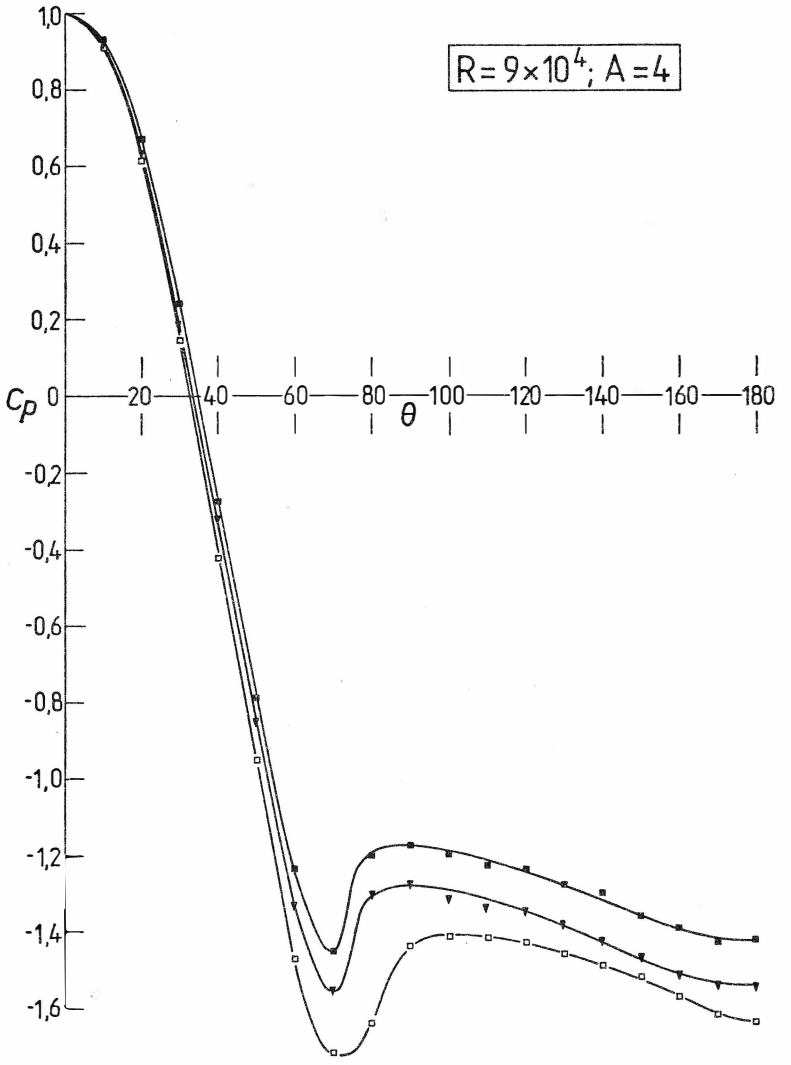

FIGURE 8.6 : Pressure distribution around cylinder. Blockage ratio: Δ, 1.2%; o, 2.4%; +, 3.5%; ●, 5.8%; ■, 9%; ▼, 12.3%; □, 15.2%.

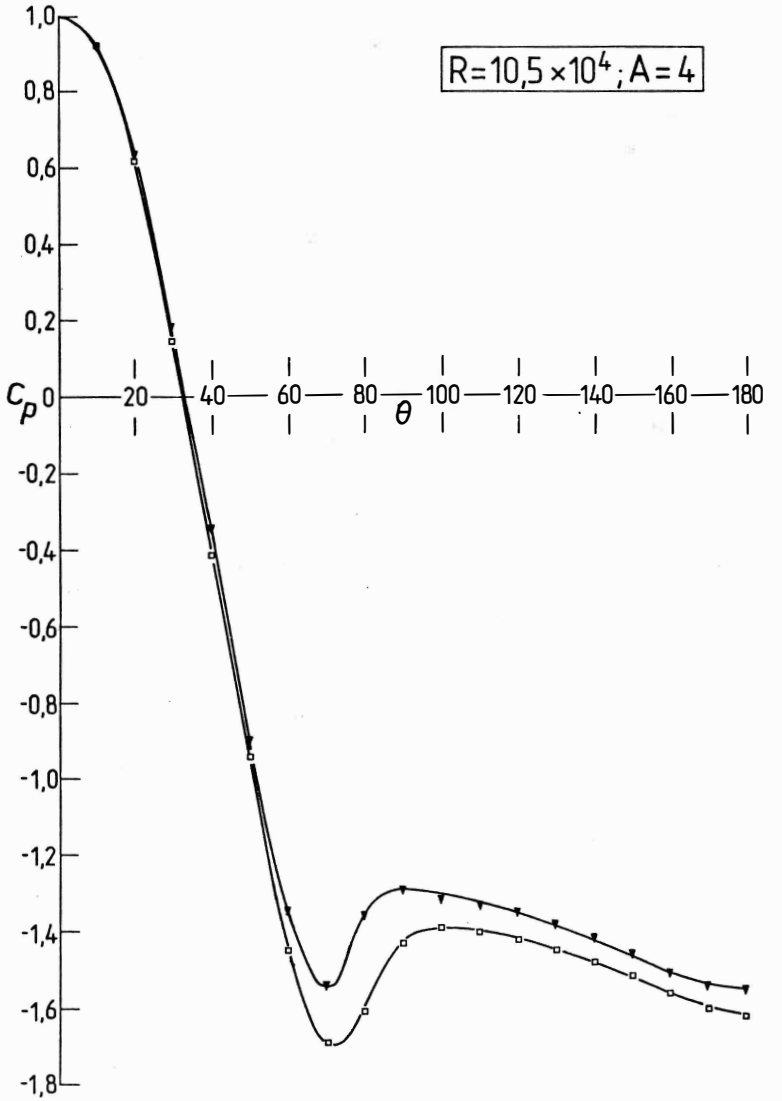

FIGURE 8.7 : Pressure distribtuin around cylinder. Blockage ratio: △, 1.2%; o, 2.4%; +, 3.5%; ●, 5.8%; ■, 9%; ▼, 12.3%; □, 15.2%.

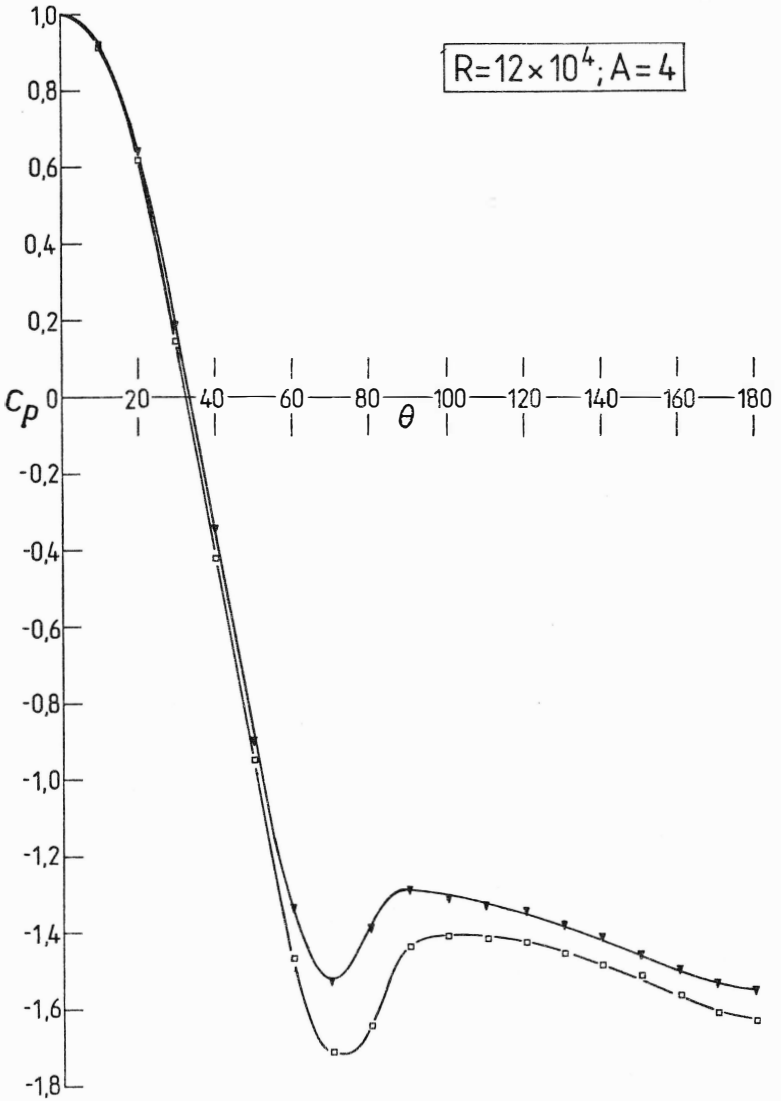

FIGURE 8.8 : Pressure distribution around cylinder. Blockage ratio: Δ, 1.2%; 0, 2.4%; +, 3.5%; ●, 5.8%; ■, 9%; ▼, 12.3%; □, 15.2%.

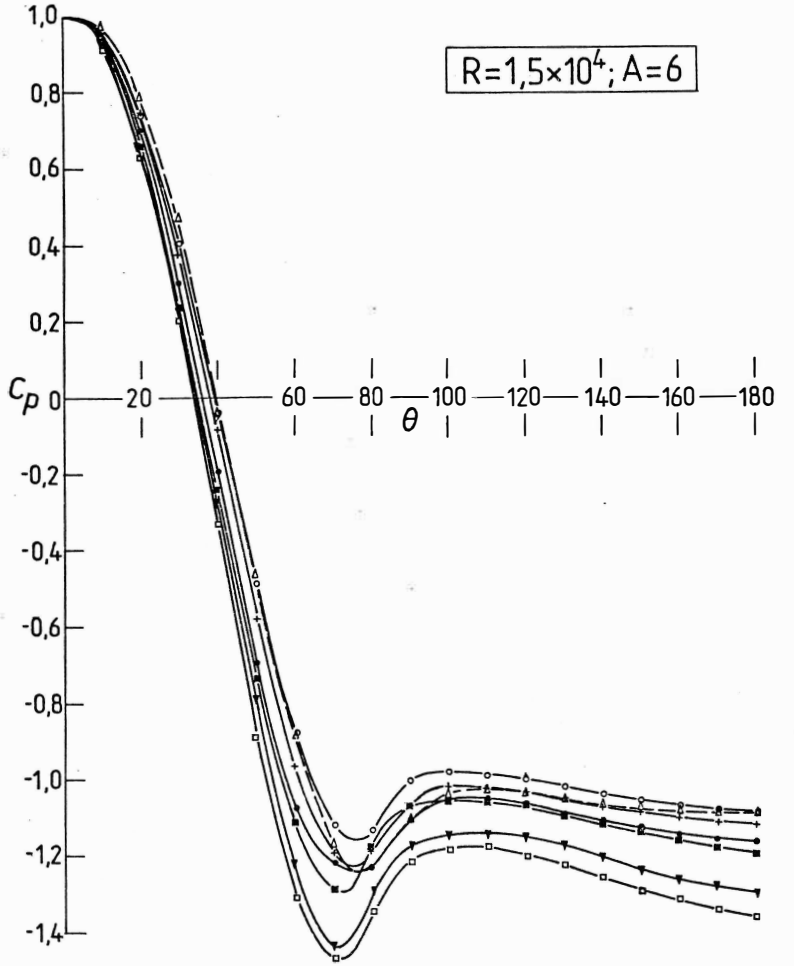

FIGURE 8.9 : Pressure distribution around cylinder. Blockage ratio: Δ, 1.2%; o, 2.4%; +, 3.5%; ●, 5.8%; ■, 9%; ▼, 12.3%; □, 15.2%.

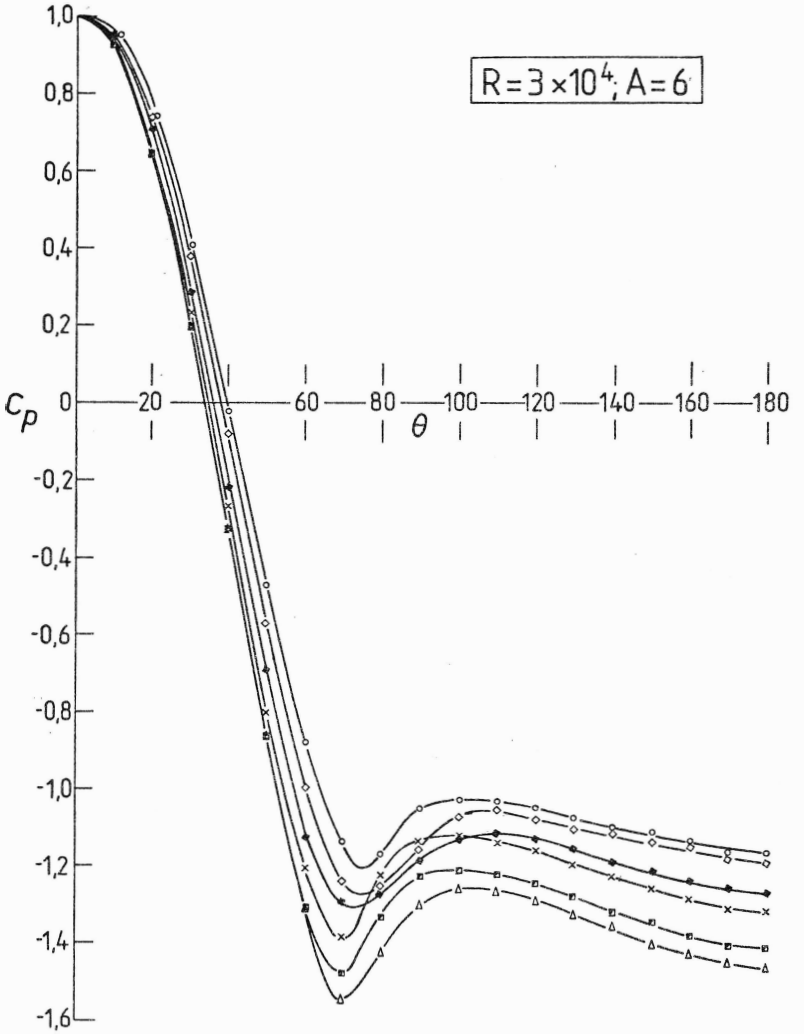

FIGURE 8.10 : Pressure distribution around cylinder. Blockage ratio: △, 1.2%; o, 2.4%; +, 2.5%; ●, 5.8%; ■, 9%; ▼, 12.3%; □, 15.2%.

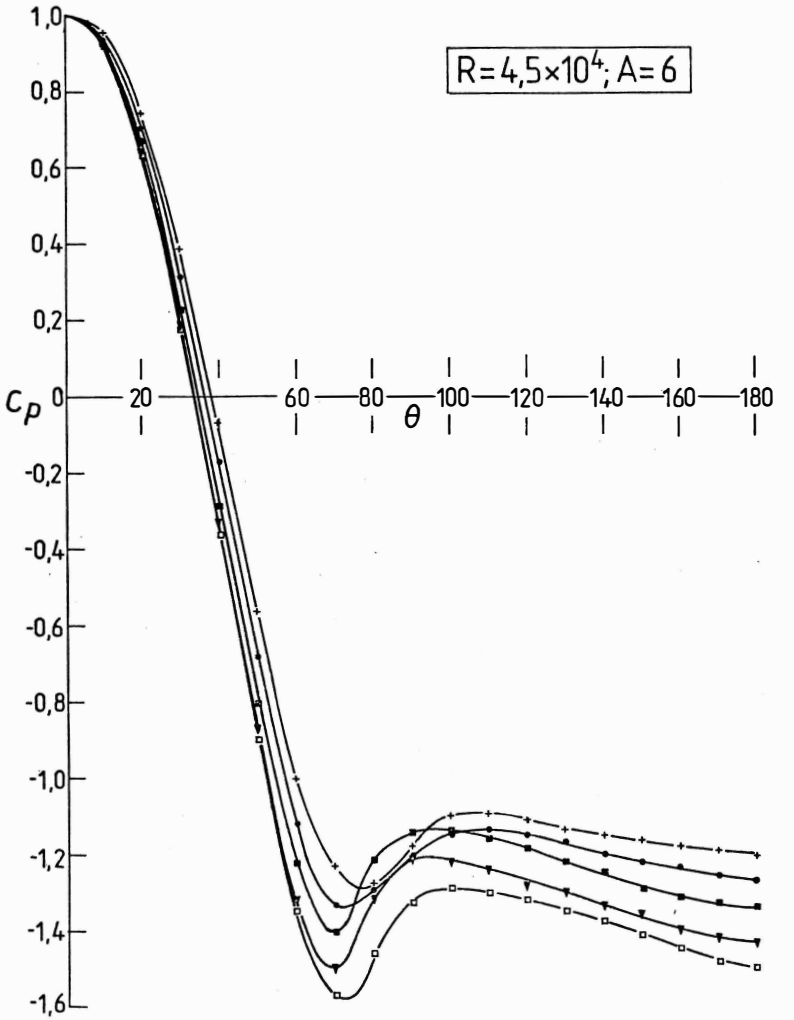

FIGURE 8.11 : Pressure distribution around cylinder. Blockage ratio: Δ, 1.2%; o, 2.4%; +, 3.5%; ●, 5.8%; ■, 9%; ▼, 12.3%; □, 15.2%.

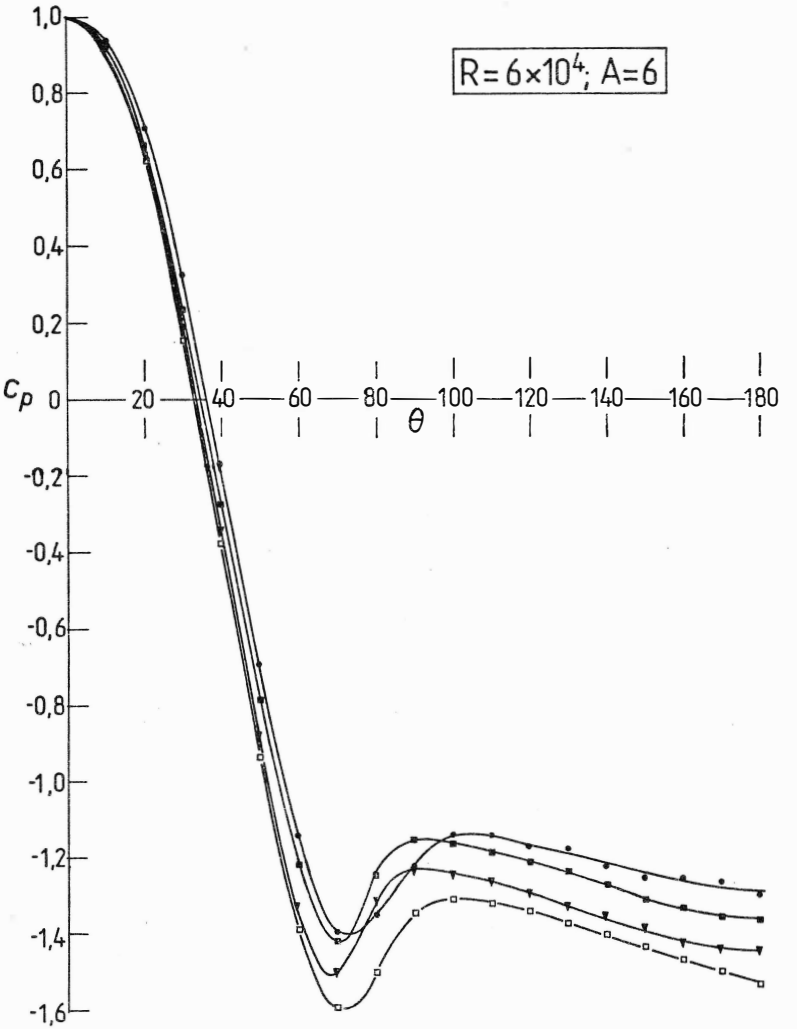

FIGURE 8.12 : Pressure distribution around cylinder. Blockage ratio: Δ, 1.2%; o, 2.4%; +, 3.5%; ●, 5.8%; ■, 9%; ▼, 12.3%; □, 15.2%.

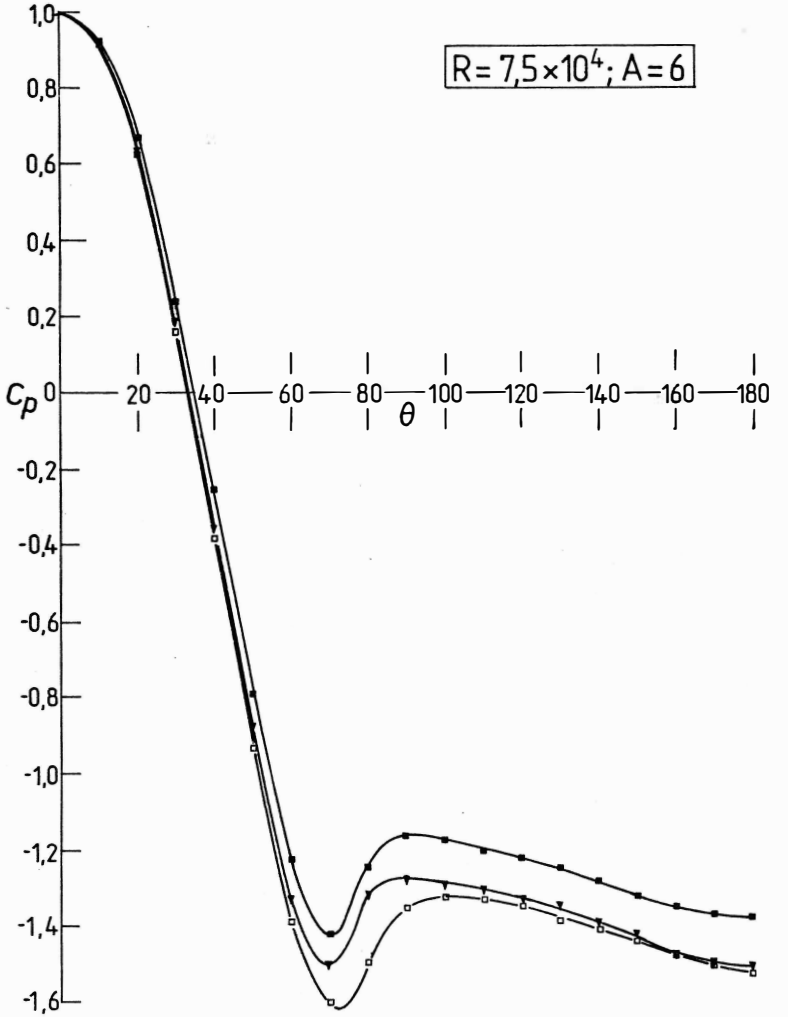

FIGURE 8.15 : Pressure distribution around cylinder. Blockage ratio: Δ, 1.2%; o, 2.4%; +, 3.5%; ●, 5.8%; ■, 9%; ▼, 12.3%, □, 15.2%.

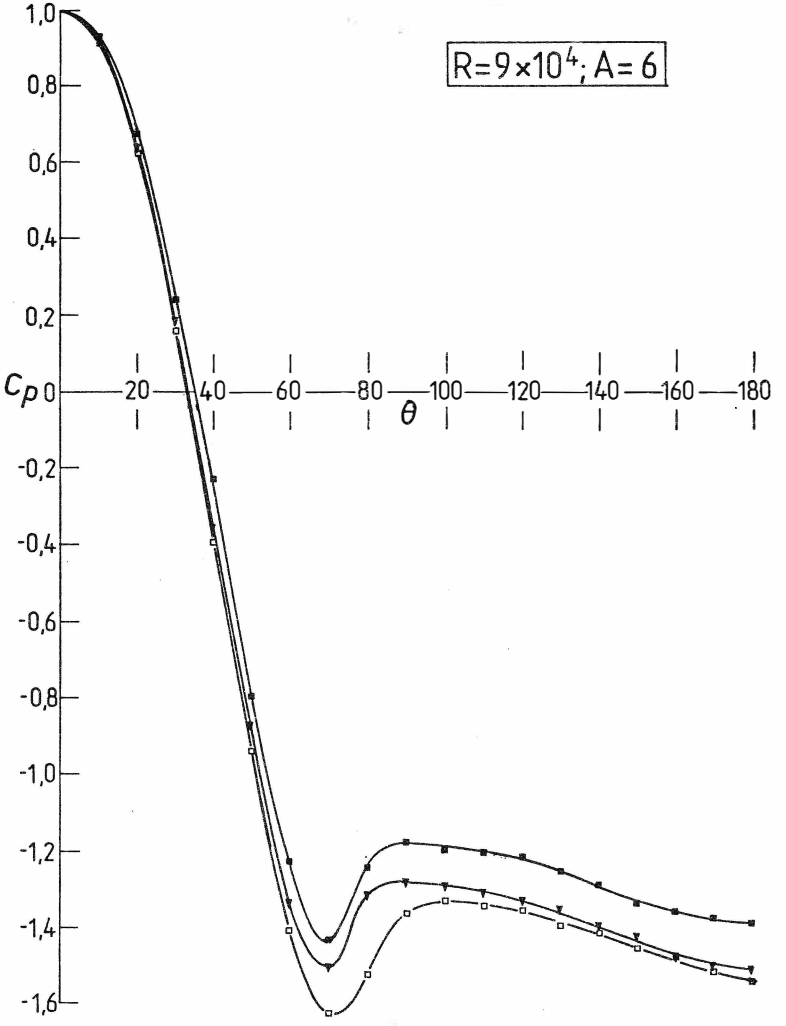

FIGURE 8.14 : Pressure distribution around cylinder. Blockage ratio: Δ, 1.2%; o, 2.4%; +, 3.5%; ●, 5.8%; ■, 9%; ▼, 12.3%; □, 15.2%.

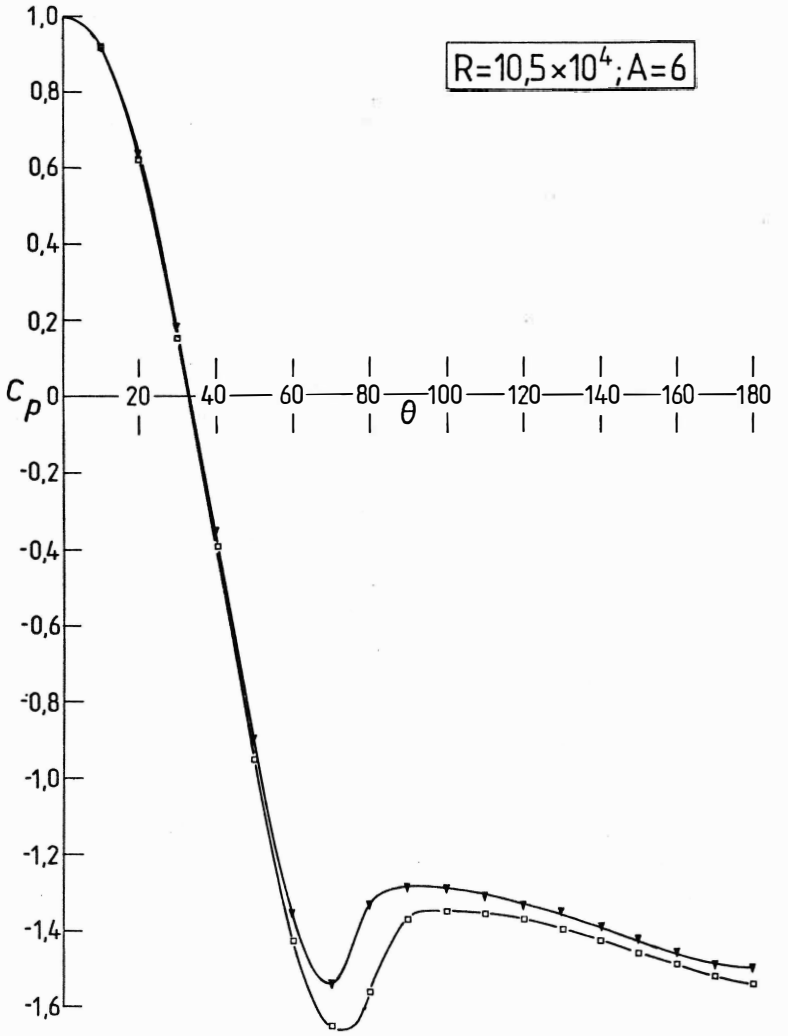

FIGURE 8.15 : Pressure distribution around cylinder. Blockage ratio: △, 1.2%; o, 2.4%; +, 3.5%; ●, 5.8%; ■, 9%; ▼, 12.3%; □, 15.2%.

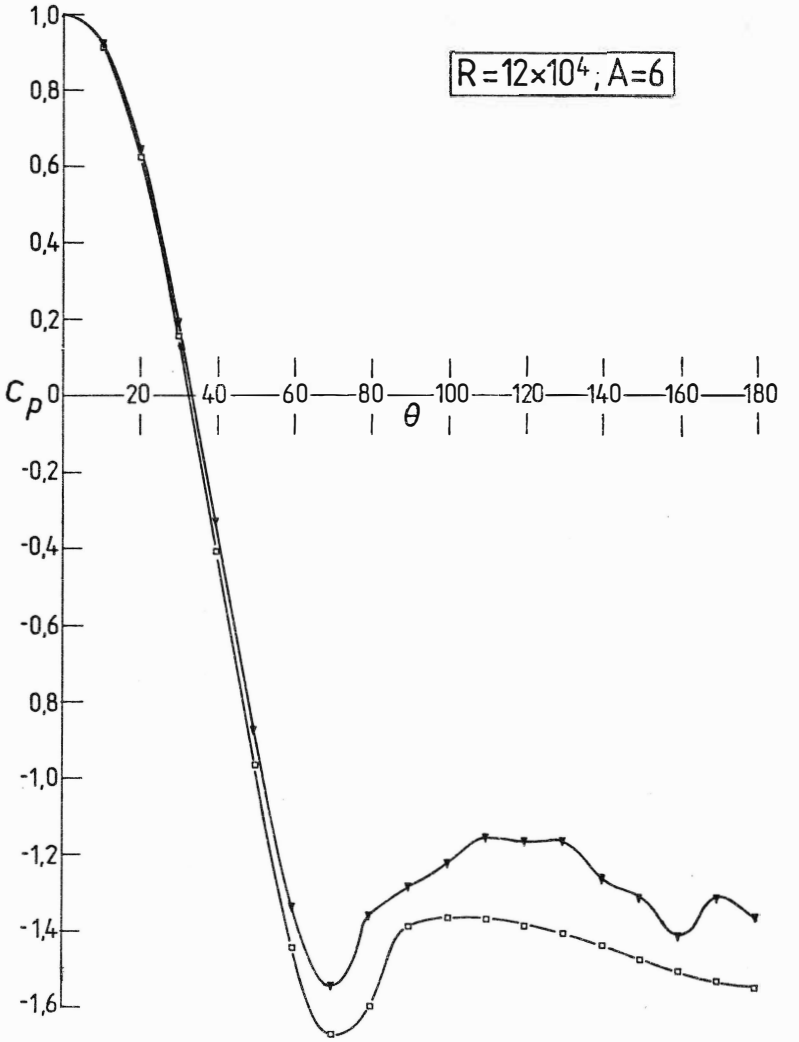

FIGURE 8.16 : Pressure distribution around cylinder. Blockage ratio: Δ, 1.2%; o, 2.4%; +, 3.5%; ●, 5.8%; ■, 9%; ▼, 12.3%; □, 15.2%.

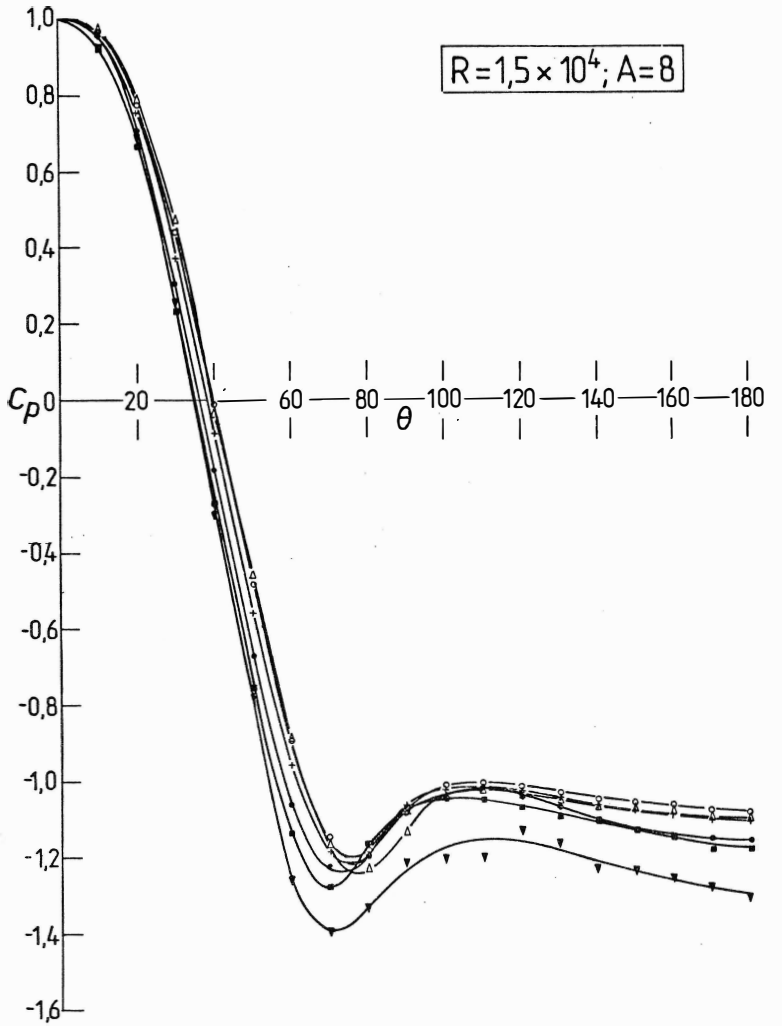

FIGURE 8.17 : Pressure distribution around cylinder. Blockage ratio: △, 1.2%; o, 2.4%; +, 3.5%; ●, 5.8%; ■, 9%; ▼, 12.3%; □, 15.2%.

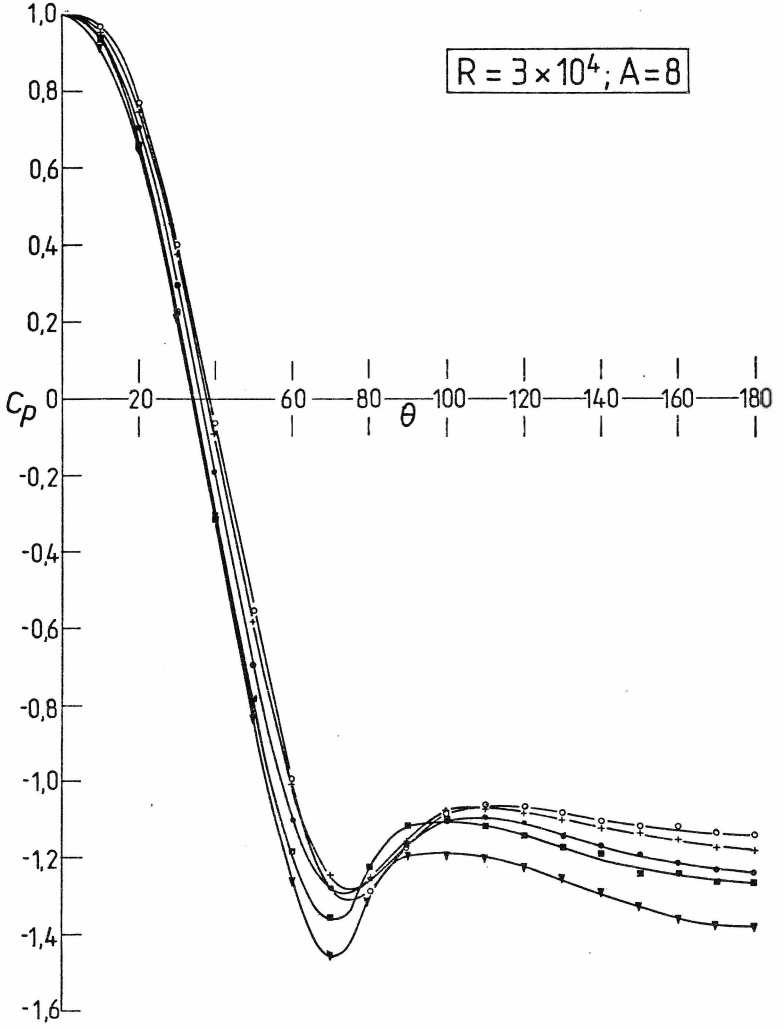

FIGURE 8.18 : Pressure distribution around cylinder. Blockage ratio: Δ, 1.2%; o, 2.4%; +, 3.5%; ●, 5.8%; ■, 9%; ▼, 12.3%; □, 15.2%.

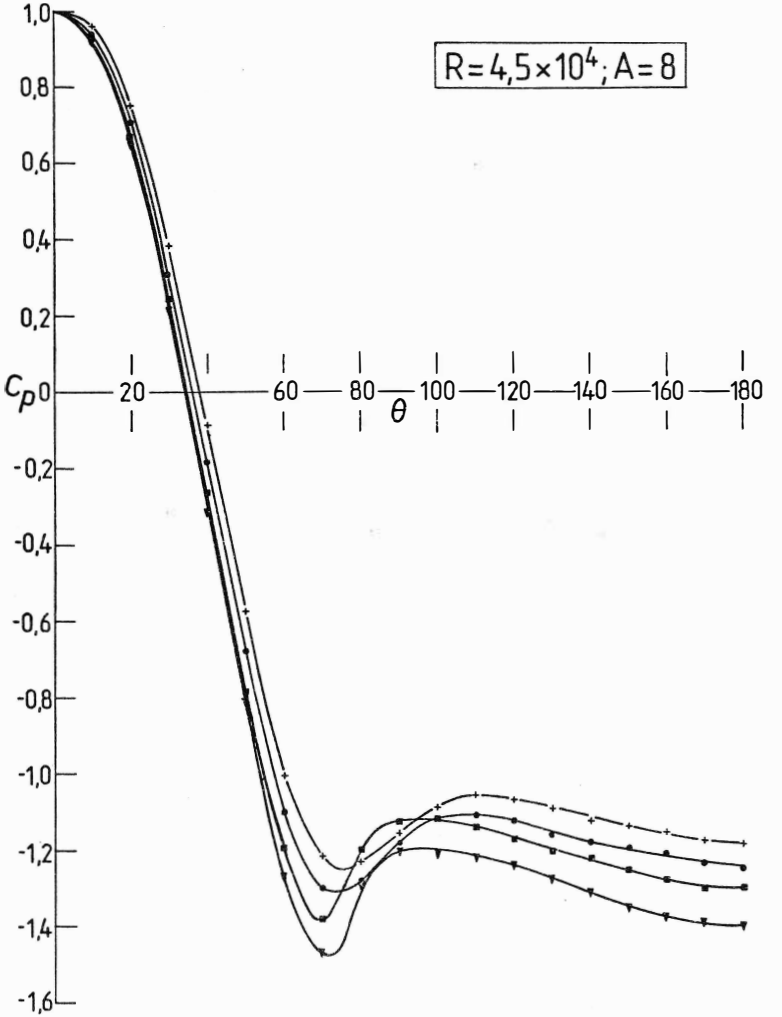

FIGURE 8.1 : Pressure distribution around cylinder. Blockage ratio: △, 1.2%; o, 2.4%; +, 3.5%; ●, 5.8%; ■, 9%; ▼, 12.3%; □, 15.2%.

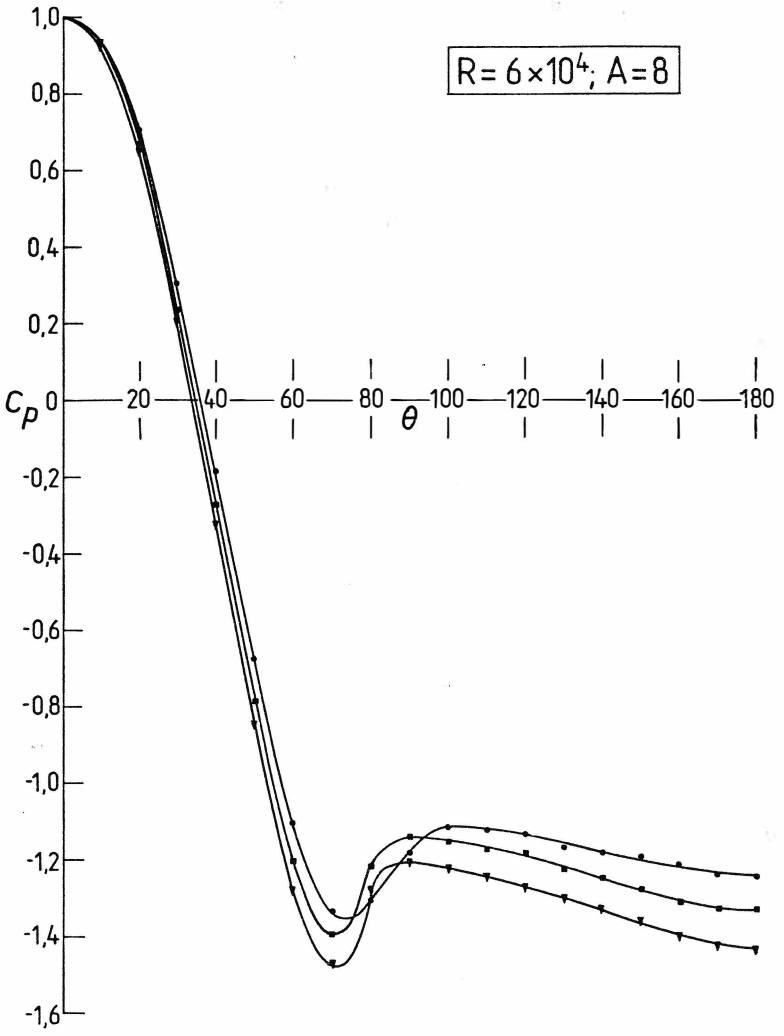

FIGURE 8.20 : Pressure distribution around cylinder. Blockage ratio: △, 1.2%; o, 2.4%; +, 3.5%; ●, 5.8%; ■, 9%; ▼, 12.3%; □, 15.2%.

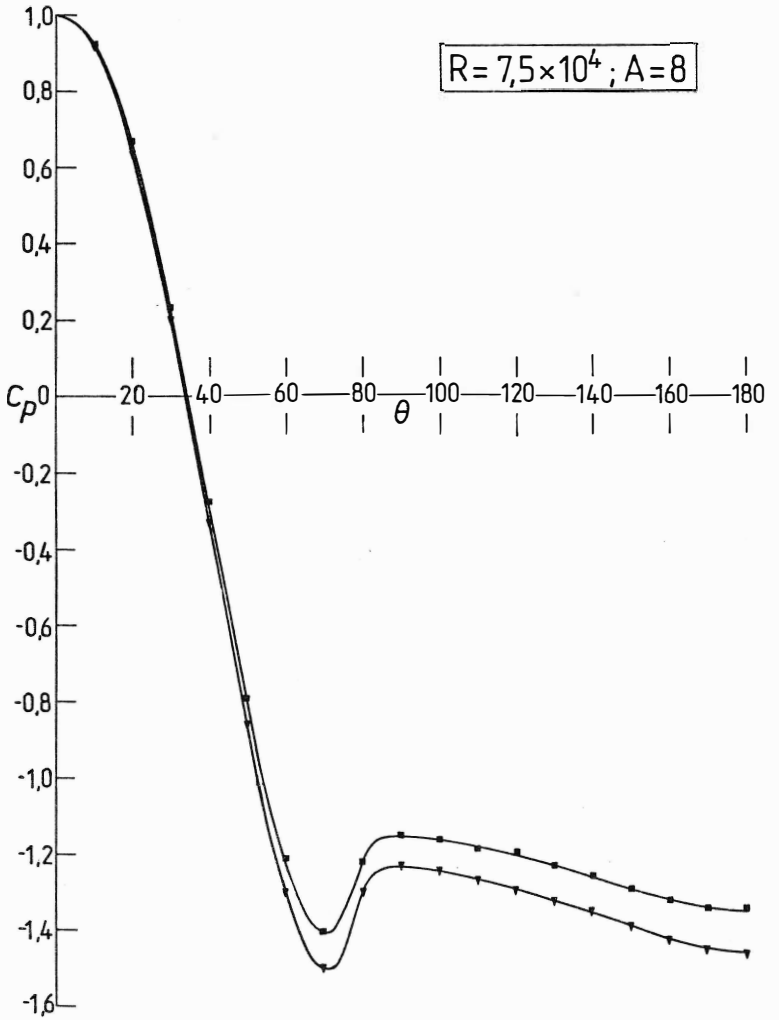

FIGURE 8.21 : Pressure distribution around cylinder. Blockage ratio: △, 1.2%; o, 2.4%; +, 3.5%; ●, 5.8%; ■, 9%; ▼, 12.3%; □, 15.2%.

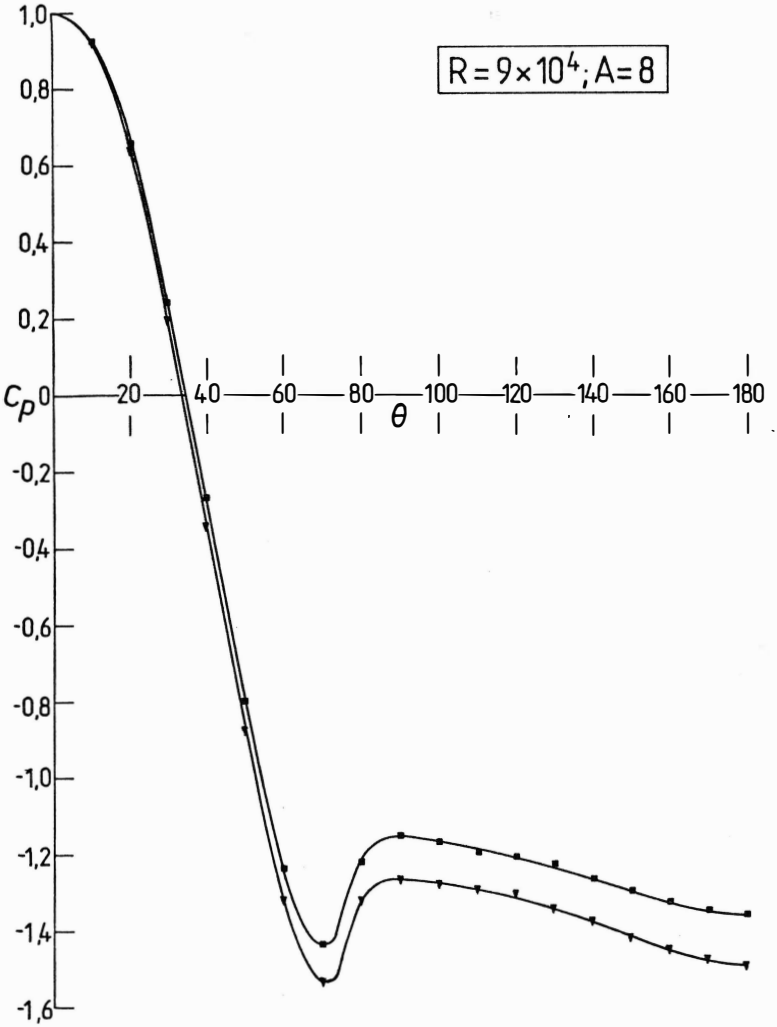

FIGURE 8.22 : Pressure distribution around cylinder. Blockage ratio: Δ, 1.2%; o, 2.4%; +, 3.5%; ●, 5.8%; ■, 9%; ▼, 12.3%; □, 15.2%.

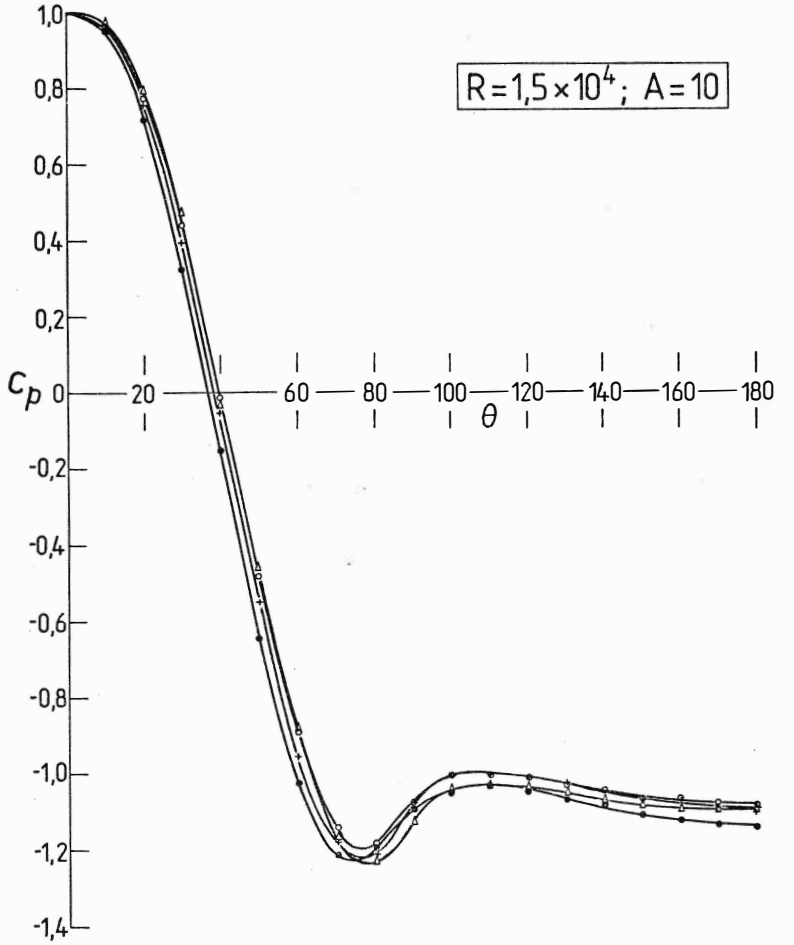

FIGURE 8.23 : Pressure distribution around cylinder. Blockage ratio: △, 1.2%; o, 2.4%; +, 3.5%; ●, 5.8%; ■, 9%; ▼, 12.3%; □, 15.2%.

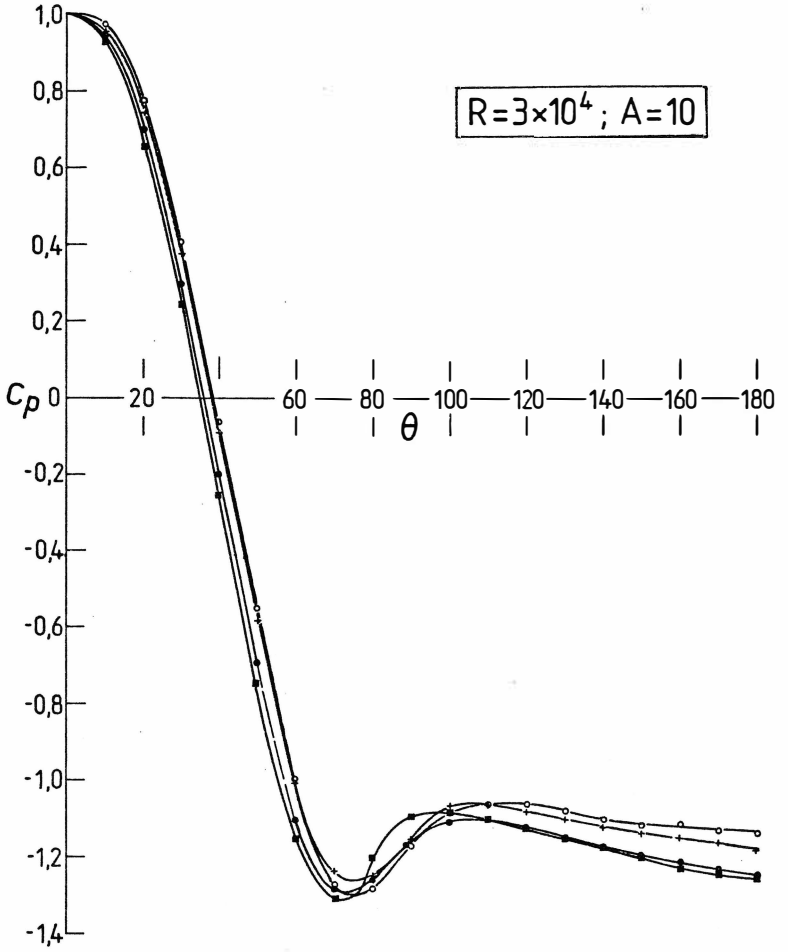

FIGURE 8.24 : Pressure distribution around cylinder. Blockage ratio: Δ, 1.2%; o, 2.4%; +, 3.5%; ●, 5.8%; ■, 9%; ▼, 12.3%; □, 15.2%.

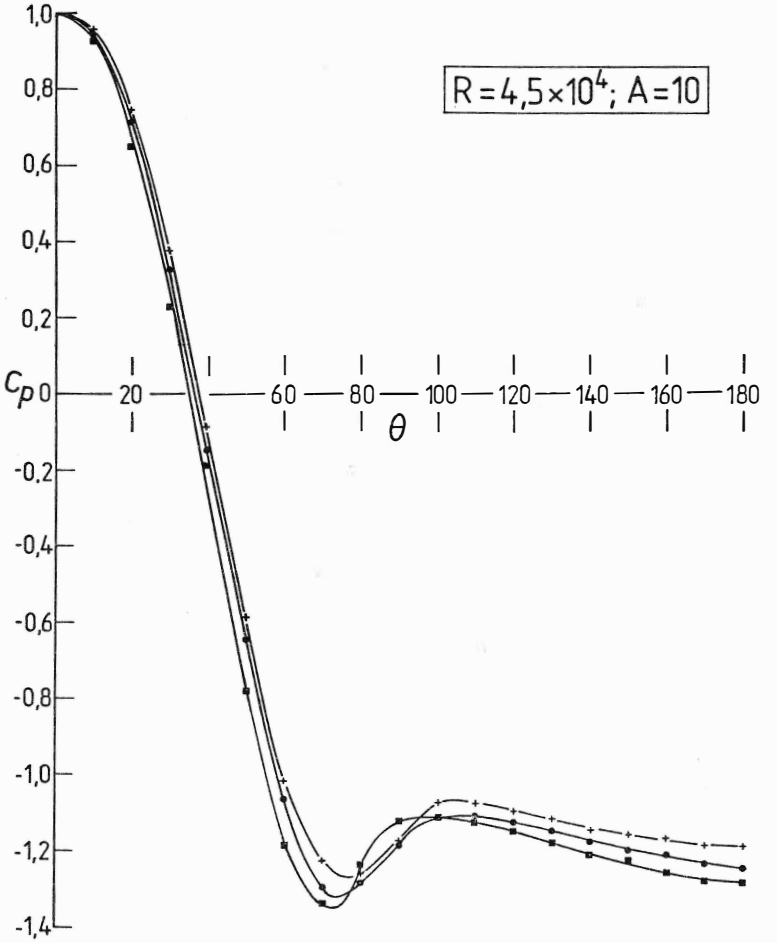

FIGURE 8.25 : Pressure distribution around cylinder. Blockage ratio: △, 1.2%; 0, 2.4%; +, 3.5%; ●, 5.8%; ■, 9%; ▼, 12.3%; □, 15.2%.

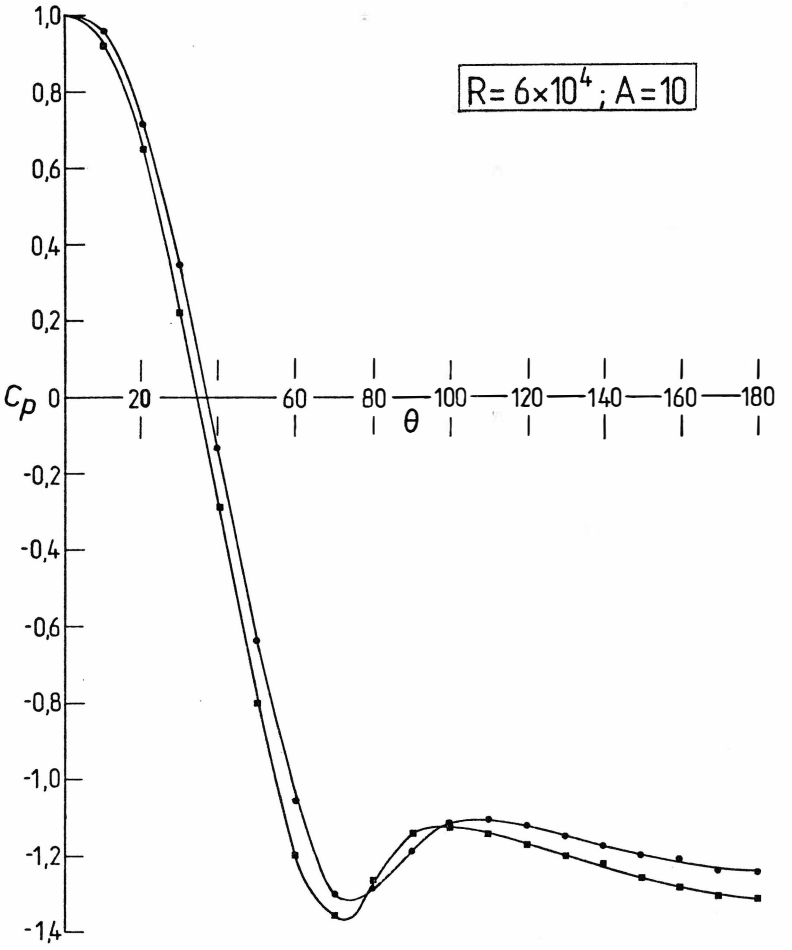

FIGURE 8.26 : Pressure distribution around cylinder. Blockage ratio: Δ, 1.2%; o, 2.4%; +, 3.5%; ●, 5.8%; ■, 9%; ▼, 12.3%; □, 15.2%.

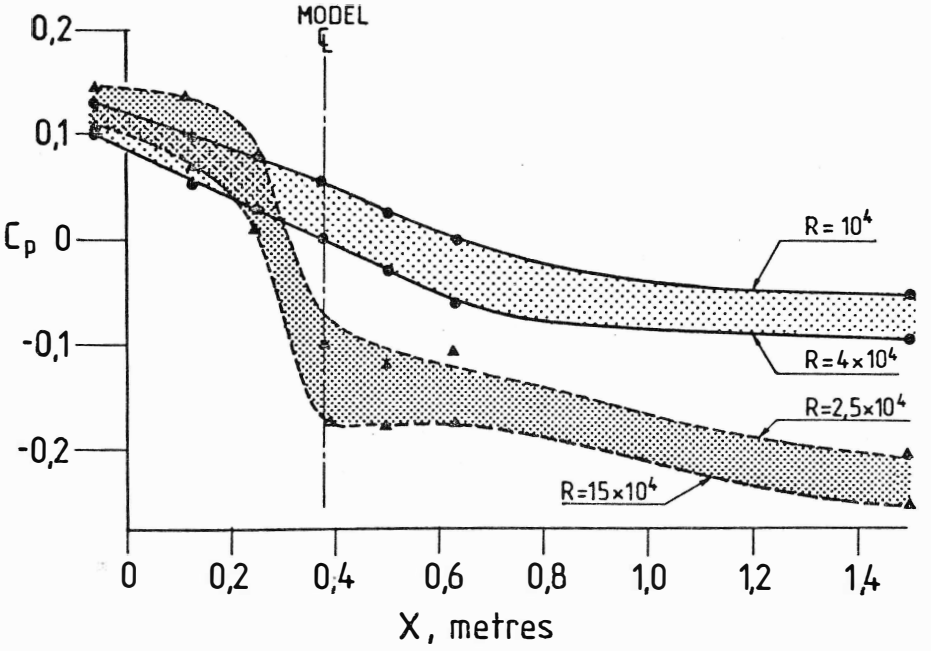

FIGURE 9 : Variation of tunnel-floor pressure coefficient along working section. Blockage ratio: ●, 6%; ▲, 16%.

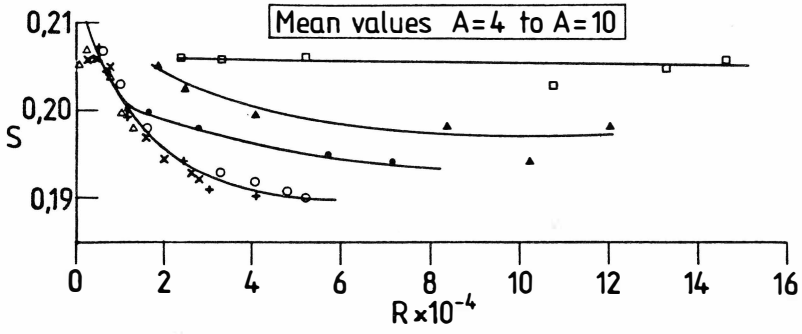

FIGURE 10 : The Strouhal-number versus Reynolds-number relationship for all aspect ratios. Blockage ratio: □, 15.5%; ▲, 12.3%; ●, 9%; o, 5.8%; +, 3.5%; x, 2.4%; Δ, 1.2%.

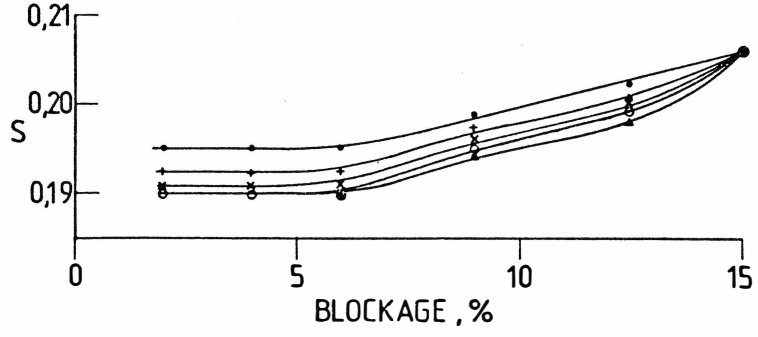

FIGURE 11 : Variation of Strouhal number with blockage. Reynolds number: o, 2 x 10^4; +, 3 x 10^4; x, 4 x 10^4; o, 5 x 10^4; Δ, 6 x 10^4.

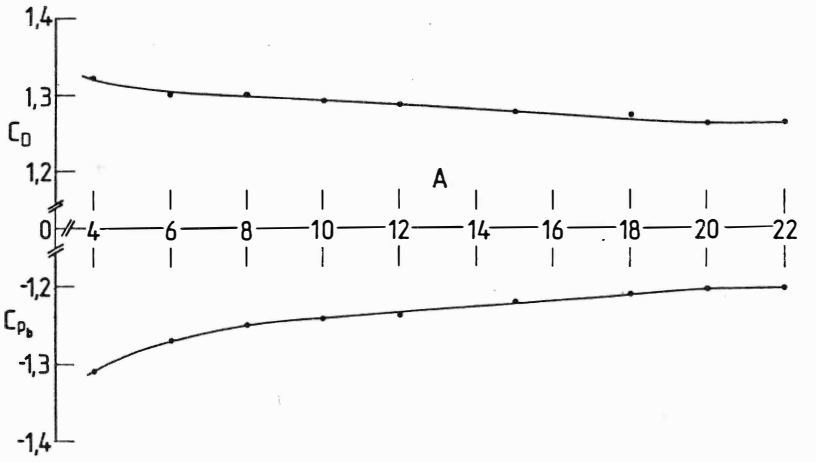

FIGURE 12 : Variation of drag coefficient and base-pressure coefficient with aspect ratio at R = 3.3 x 10^4 and blockage ratio, 6%.

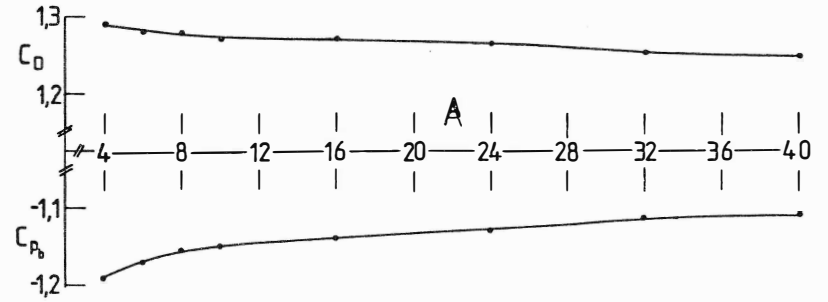

FIGURE 13 : Variation of drag coefficient and base pressure coefficient with aspect ratio at R = 2.2 x 10^4 and blockage ratio 3.5%.

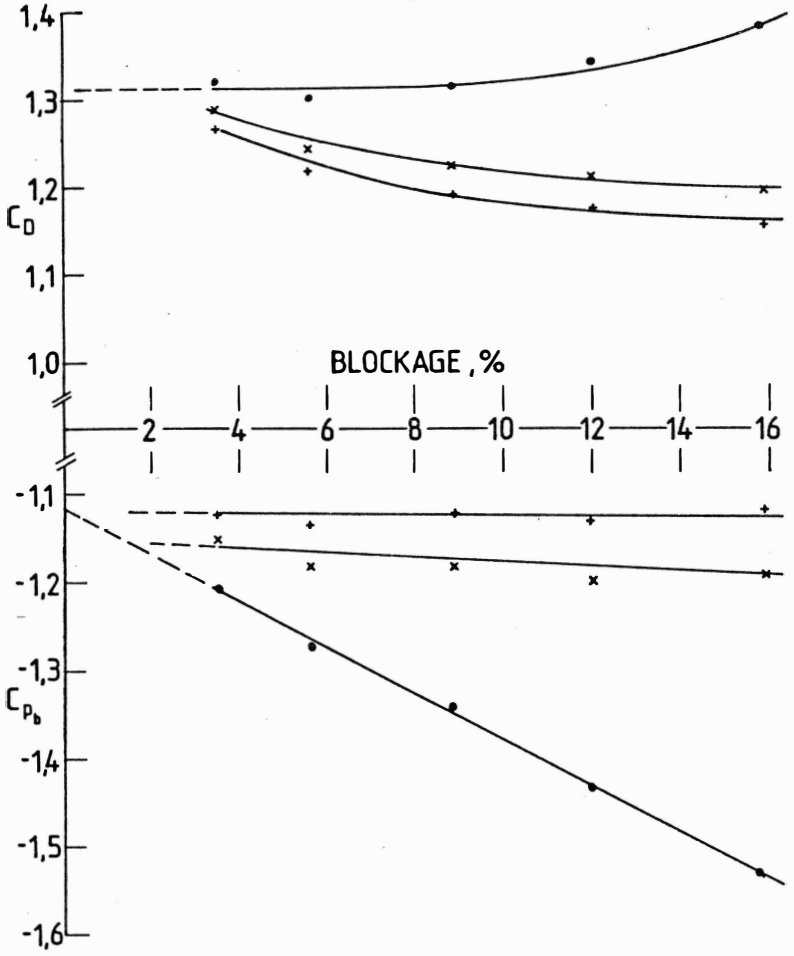

FIGURE 14 : 'Image' and 'momentum' corrections compared with measured values at A = 6, R = 4.5 x 10^4.
o, measured data; x, corrected by image method;
+, corrected by momentum method.

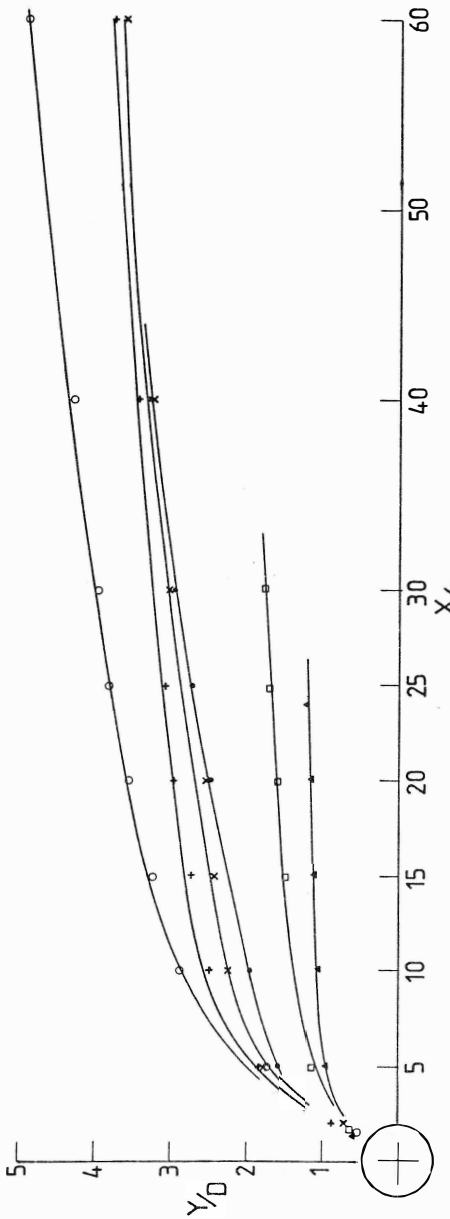

FIGURE 15 : Wake profiles at R = 2.75 x 10^4. Blockage ratio: ●, 2.3%; +, 3.5%; x, 6%; o, 9%, □, 12.5%; ▲, 16%.

5. DISCUSSION

The results show how drag coefficient, base-pressure coefficient and Strouhal number are affected by blockage, aspect ratio and Reynolds number. Since the Reynolds number effect is already well documented (see, for example, Morkovin 1964; Lienhard 1966) the following discussion concentrates on the blockage and aspect-ratio effects.

5.1 Blockage Effects

Figures 8 provide a clear demonstration of the effects of blockage on pressure distribution, all other parameters being held constant. Three regions can be distinguished around the cylinder; (a) from 0 to 7^{o}, (b) from 70 to 120^{o}, (c) from 120 to 180^{o}. Increasing blockage progressively lowers pressures in regions (a) and (c) but produces two different patterns in region (b) depending on whether blockage is less than or greater than about 6%. This distinct change in shape of the pressure distribution which occurs when the blockage is increased above 6% was observed in the series of tests for all aspect ratios and over the range of Reynolds number in which enough data were available for comparison, i.e. 10^{4} to 6×10^{4}. If it is assumed that the mean position of the separation point is indicated by the location of the region of adverse pressure gradient downstream from the point of minimum pressure, it appears from the pressure distributions of Figure 8 that, as the blockage is increased from small values up to 6%, the separation point is moved slightly downstream. However, as the blockage is increased between 6 and 9% there appears to be a relatively rapid shift upstream of the separation point which then remains unchanged as the blockage is increased further up to 16%.

It is obvious that no simple blockage correction procedure can be used correctly in such a situation where the actual shape of the pressure distribution changes with blockage. A simple correction procedure for regions (a) and (c) can be envisaged to predict the unblocked pressure field but not in region (b), in the vicinity of separation, where changes are much more complex. As far as drag is concerned,

the effects of changes in pressure distribution in regions (a) and (c) are of opposite sign, reduced pressure decreasing the drag contribution of (a) but increasing that of (c). These changes are of the same order of magnitude so that the change of total drag coefficient is governed largely by events in region (b). Figure 6 shows that, whereas C_{p_b} and $C_{D(90-180)}$ are almost linear functions of blockage, C_D hardly varies at all.

The commonly used blockage correction procedures based on the image concept (Allen and Vincenti 1944) or the momentum concept (Maskell 1963) do not take into account the changes in the pressure field described above. Hence, they are particularly inappropriate for region (b) where the form of the pressure distribution changes with blockage but, in the base region, where the form, but not the magnitude, of the pressure distribution does not vary markedly with blockage, these procedures are more effective. Consequently, they cannot adequately correct the drag coefficient for cases where the form of the pressure distribution varies with blockage.

In the appendix an example is presented in which these two correction procedures are applied to the circular cylinder with aspect ratio 6 at Reynolds number 4.5×10^4. The results of these correction procedures are summarized in Figure 14. The momentum method predicts the unblocked base pressure coefficient from the measured data quite well. However, both procedures are unsatisfactory in their prediction of the unblocked drag coefficient and the 'corrected' values are, in fact, worse than the uncorrected experimental data. These results are typical.

It is of general interest, although not strictly relevant to this paper, to point out that these corrections are more effective for bluff profiles with fixed separation points than for rounded profiles. A separate investigation (West 1981) has shown that the momentum method, at least, is very effective in correcting both pressure and drag coefficients for the former profiles.

The wake frequencies, presented as Strouhal numbers in Figures 10 and 11, also react differently with blockage ratios below and above 6%. Below 6% a unique relationship between Strouhal number and Reynolds number exists for all blockage ratios; above 6% the Strouhal number, at a given Reynolds number, rises rapidly with blockage and at 16% it is apparently invariant with Reynolds number. However, it is uncertain what would occur at even higher blockage. The increase in Strouhal number for blockage ratios from 6 to 16% is clearly associated with the upstream movement of the separation point with increasing blockage, evident from the pressure distributions in Figures 8.

Tunnel-floor pressures, Figure 9, reflect the distortion of the pressure distribution around the cylinder, noted in Figures 8. For blockage up to 6% the variation of pressure along the working section is fairly uniform but, for larger blockage, increasingly steep pressure gradients occur in the vicinity of the cylinder as the pressure distribution in region (b) on the cylinder is distorted.

The tunnel-floor pressures shown in Figure 9 provide some insight into the reason for the changes in the location of the separation point on the cylinder. For blockage ratios up to 6% there is nearly uniform favourable pressure gradient imposed on the flow field for considerable distances upstream and downstream from the cylinder. This should have a beneficial, though small, effect on the velocity profile in the laminar boundary layer on the cylinder thus enabling the separation point to move slightly downstream. However, for blockage ratios greater than 6% the favourable pressure gradient, though larger, now terminates at the location of the maximum width of the cylinder and downstream from here the tunnel-floor pressure is effectively constant. It is suggested that this could explain the sudden shift upstream of the separation point on the cylinder when the blockage ratio is increased from 6 to 9%.

5.2 Aspect-Ratio Effects

Changes in aspect ratio at constant blockage have no

effect on Strouhal number, the data for Figure 10 having been obtained at all aspect ratios between 4 and 10.

The drag coefficient and base-pressure coefficient vary smoothly with aspect ratio as shown in Figures 12 and 13. The base-pressure coefficient increases and the drag coefficient decreases correspondingly as the aspect ratio is increased. The changes are relatively rapid as the aspect ratio increases from small values but they become smaller and smaller as, at large aspect ratios, the curves approach asymptotes appropriate to an infinitely long cylinder. It is noted that, while the changes of C_D and C_{p_b} are small for $A > 20$, nevertheless, small changes could still be detected up to $A = 40$, the largest value attainable in this experiment.

It is noted that reduction in aspect ratio has similar effects on C_D and C_{p_b} as does increase in blockage. It is this which makes it so important to control both parameters if an accurate description of blockage effects is sought.

In all of these experiments, the cylinders were fitted with geometrically similar end-plates. Within the accuracy of measurement (a fraction of one per cent) the end-plates achieve spanwise uniformity of mean conditions by preventing the three-dimensional flow which would otherwise occur where the cylinder meets the tunnel wall. However, the end-plates unavoidably introduce 'second-order' end effects because of the boundary layer which must form on them. This boundary layer, largely laminar, is very much thinner than that existing on the tunnel wall, but nevertheless, it appears to have effects which are measurable up to $A = 40$, as shown in Figure 13. It is possible that three-dimensional structures in the wake also contribute to these second-order effects.

The studies by Modi and El-Sherbiny (1971) of the effects of wall confinement on flow past circular cylinders were carried out in the same range of Reynolds number as the experiments reported here; however, they covered a larger range of blockage. The experimental results they obtained appear to be generally similar to those presented here. However, regrettably, they did not control the aspect ratio in their experiments nor did

they use end plates; each cylinder tested spanned the width of the tunnel working section, so that the aspect ratio varied as the blockage ratio varied. Consequently their results contain the combined effects of variations of blockage ratio and of apsect ratio and it is not possible to separate the two effects. The results reported in this paper, which were obtained with both parameters being controlled separately, do not support that conclusion of Modi and El-Sherbiny which stated that correction procedures based on the image method and on the momentum method are effective at lower 'bluffness' (blockage ratios).

The experiments reported by Farell *et al.* (1977) were carried out on roughened cylinders at generally larger Reynolds numbers than those for the experiments reported here. Consequently, no direct comparison can be made betwen the two sets of experiments.

6. CONCLUSIONS

(1) The data presented give comprehensive information on the flow parameters for flow past a circular cylinder within the range $10^4 < R < 10^5$. Strict attention to detail has resulted in accurate and comparable results.

(2) If the blockage is less than 6%, the shape of the pressure distribution around the circular cylinder varies only slightly with blockage and the Strouhal number is independent of both the blockage ratio and the aspect ratio.

(3) For blockage ratios in the range 6 - 16%, there is considerable distortion of the flow compared with that of the unblocked state. The effects of blockage are complex the pressure distribution is of a distinctly different form and the Strouhal number changes with blockage ratio, but conflicting influences in the pressure distribution result in a measured (blocked) drag coefficient which is not much different from that for no blockage. It is unlikely that a simple blockage correction procedure applicable to all these quantities exists.

(4) The simple blockage procedures based on the momentum

method and on the image method are quite unsatisfactory in their prediction of the unblocked drag coefficient. However, the momentum method predicts the unblocked base-pressure coefficient quite well.

(5) Reduction in aspect ratio has effects on drag coefficient and on base-pressure coefficient which are similar to those associated with increase in blockage ratio and it is essential to control both parameters separately in order to obtain an accurate description of the effects of either.

(6) Even when end plates are used the flow past a cylinder with finite aspect ratio is not strictly two-dimensional. Although the effects due to aspect ratio are not large for $A > 20$, small influences can be detected up to aspect ratios of 40.

APPENDIX A - BLOCKAGE CORRECTIONS

Table 2 and Figure 14 show typical results for the particular case A = 6, R = 4.5×10^4 together with corrected values based on the 'image' and 'momentum' concepts.

(a) *Image method:*

$$\frac{C_{dc}}{C_d} = \frac{1}{(1+e)^2} = \frac{1 - C_{pc}}{1 - C_p}$$

Subscript c indicates a corrected value and e is the approach flow velocity increment to allow for solid blockage and wake blockage (Pankhurst and Holder, 1952):

$$e = \frac{\pi^2}{12}(B)^2 + \frac{C_d}{4}(B).$$

TABLE 2: Effects of tunnel blockage on flow past a cylinder. A = 6, R = 4.5×10^4

Model		Measured Values		Corrected Values			
				Image Method		Momentum Method	
Dia. (mm)	Blockage (%)	C_p	C_{Pb}	C_D	C_{Pb}	C_D	C_{Pb}
9.5	3.5	1.321	- 1.210	1.288	- 1.156	1.269	- 1.123
12.6	5.7	1.300	- 1.275	1.247	- 1.181	1.220	- 1.136
22.2	8.9	1.315	- 1.342	1.226	- 1.183	1.191	- 1.121
31.8	12.0	1.343	- 1.435	1.213	- 1.200	1.176	- 1.131
41.2	15.8	1.381	- 1.534	1.195	- 1.192	1.156	- 1.121

(b) *Momentum method:*

$$\frac{C_{d_c}}{C_d} = 1 - m(B) = \frac{kc^2}{k^2} = \frac{1 - C_{Pb_c}}{1 - C_{P_b}}$$

where kc is found by iteration from the measured base pressure;

$$C_{P_b} = 1 - k^2.$$

MODEL DIAMETER: 6.4 mm BLOCKAGE: 2.4%

R ÷ 10^4	A	C_d	C_p																	
			0°	10°	20°	30°	40°	50°	60°	70°	80°	90°	100°	110°	120°	130°	140°	150°	160°	170°	180°
1.5	4	1.257	+1	+ .944	+ .734	+ .380	- .040	- .511	- .905	-1.153	-1.140	- .988	- .992	-1.013	-1.024	-1.043	-1.064	-1.087	-1.102	-1.119	-1.122
3	4	1.295	+1	+ .948	+ .743	+ .399	- .036	- .49	- .891	-1.160	-1.182	-1.055	-1.033	-1.036	-1.053	-1.081	-1.103	-1.115	-1.135	-1.145	-1.150
1.5	6	1.245	+1	+ .943	+ .739	+ .405	- .033	- .486	- .880	-1.122	-1.136	-1.005	- .986	- .997	-1.006	-1.024	-1.043	-1.060	-1.073	-1.085	-1.094
3	6	1.305	+1	+ .948	+ .749	+ .405	- .024	- .469	- .880	-1.139	-1.170	-1.050	-1.027	-1.031	-1.052	-1.073	-1.093	-1.111	-1.138	-1.157	-1.161
1.5	8/10	1.259	+1	+ .961	+ .774	+ .439	- .014	- .484	- .891	-1.148	-1.181	-1.080	-1.015	-1.010	-1.016	-1.031	-1.050	-1.058	-1.066	-1.080	-1.090
3	8/10	1.277	+1	+ .974	+ .775	+ .402	- .063	- .550	- .995	-1.279	-1.287	-1.178	-1.085	-1.066	-1.068	-1.082	-1.106	-1.120	-1.117	-1.133	-1.140

MODEL DIAMETER: 3.2 mm BLOCKAGE: 1.2%

R ÷ 10^4	A	C_d	C_p																	
			0°	10°	20°	30°	40°	50°	60°	70°	80°	90°	100°	110°	120°	130°	140°	150°	160°	170°	180°
0.25	4/6/8/10	1.02	+1	+ .978	+ .825	+ .520	+ .138	- .278	- .650	- .918	- .950	- .755	- .718	- .712	- .705	- .700	- .695	- .697	- .700	- .700	- .700
0.5	4/6/8/10	1.08	+1	+ .978	+ .817	+ .500	+ .080	- .352	- .760	-1.030	-1.023	- .840	- .805	- .800	- .800	- .800	- .800	- .800	- .800	- .800	- .800
1	4/6/8/10	1.21	+1	+ .976	+ .808	+ .475	+ .043	- .419	- .856	-1.141	-1.206	-1.073	- .957	- .948	- .951	- .957	- .965	- .974	- .986	- .979	- .989
1.5	4/6/8/10	1.30	+1	+ .978	+ .798	+ .475	+ .033	- .460	- .882	-1.168	-1.231	-1.133	-1.042	-1.031	-1.039	-1.051	-1.070	-1.074	-1.084	-1.095	-1.096

MODEL DIAMETER: 9.5 mm BLOCKAGE: 3.5%

R ÷ 10^4	A	C_d	C_p																	
			0°	10°	20°	30°	40°	50°	60°	70°	80°	90°	100°	110°	120°	130°	140°	150°	160°	170°	180°
1.5	4	1.261	+1	+ .965	+ .739	+ .376	- .096	- .558	- .980	-1.211	-1.236	-1.105	-1.048	-1.033	-1.044	-1.066	-1.090	-1.109	-1.126	-1.139	-1.147
3	4	1.300	+1	+ .956	+ .734	+ .361	- .113	- .600	-1.036	-1.274	-1.290	-1.193	-1.100	-1.090	-1.110	-1.135	-1.156	-1.178	-1.200	-1.218	-1.231
4.5	4	1.325	+1	+ .956	+ 744	+ .369	- .101	- .622	-1.048	-1.270	-1.310	-1.209	-1.114	-1.108	-1.129	-1.153	-1.178	-1.193	-1.213	-1.239	-1.236
1.5	6	1.247	+1	+ .958	+ .747	+ .376	- .080	- .572	- .969	-1.191	-1.195	-1.074	-1.021	-1.020	-1.035	-1.058	-1.076	-1.093	-1.106	-1.123	-1.123
3	6	1.295	+1	+ .955	+ .748	+ .380	- .088	- .579	-1.003	-1.248	-1.262	-1.165	-1.098	-1.072	-1.086	-1.119	-1.129	-1.148	-1.162	-1.184	-1.191
4.5	6	1.321	+1	+ .955	+ .751	+ .380	- .068	- .570	-1.004	-1.235	-1.279	-1.180	-1.102	-1.098	-1.120	-1.140	-1.159	-1.170	-1.186	-1.199	-1.210
1.5	8	1.237	+1	+ .957	+ .747	+ .372	- .078	- .560	- .956	-1.182	-1.198	-1.063	-1.027	-1.022	-1.027	-1.044	-1.062	-1.080	-1.093	-1.102	-1.117
3	8	1.288	+1	+ .957	+ .749	+ .375	- .093	- .586	-1.007	-1.240	-1.251	-1.155	-1.077	-1.070	-1.086	-1.107	-1.127	-1.139	-1.157	-1.178	-1.187
4.5	8	1.288	+ 1	+ .960	+ .742	+ .380	- .081	- .570	-1.002	-1.218	-1.238	-1.167	-1.077	-1.066	-1.075	-1.099	-1.126	-1.140	-1.155	-1.180	-1.188
1.5	10	1.235	+1	+ .958	+ .754	+ .395	- .059	- .555	- .959	-1.189	-1.214	-1.074	-1.012	-1.012	-1.022	-1.036	-1.057	-1.070	-1.084	-1.095	-1.100
3	10	1.286	+1	+ .957	+ .746	+ .376	- .092	- .580	-1.004	-1.237	-1.253	-1.160	-1.074	-1.068	-1.081	-1.104	-1.125	-1.140	-1.158	-1.172	-1.182
4.5	10	1.297	+1	+ .954	+ .747	+ .377	- .088	- .585	-1.014	-1.227	-1.260	-1.172	-1.075	-1.071	-1.092	-1.114	-1.143	-1.154	-1.167	-1.185	-1.190

MODEL DIAMETER: 12.6 mm BLOCKAGE: 5.8%

R ÷ 10^4	A	C_d	C_p																	
			0°	10°	20°	30°	40°	50°	60°	70°	80°	90°	100°	110°	120°	130°	140°	150°	160°	170°	180°
1.5	4	1.269	+1	+ .948	+ .715	+ .317	- .164	- .648	-1.066	-1.252	-1.254	-1.149	-1.096	-1.084	-1.095	-1.113	-1.137	-1.160	-1.185	-1.204	-1.222
3	4	1.322	+1	+ .945	+ .706	+ .290	- .204	- .690	-1.135	-1.325	-1.314	-1.223	-1.166	-1.145	-1.159	-1.188	-1.224	-1.243	-1.269	-1.295	-1.310
4.5	4	1.332	+1	+ .943	+ .708	+ .306	- .182	- .673	-1.117	-1.341	-1.334	-1.248	-1.163	-1.150	-1.164	-1.194	-1.221	-1.248	-1.265	-1.296	-1.322
6	4	1.340	+1	+ .941	+ .705	+ .306	- .188	- .691	-1.127	-1.375	-1.367	-1.263	-1.172	-1.168	-1.177	-1.212	-1.242	-1.266	-1.277	-1.310	-1.344
1.5	6	1.230	+1	+ .950	+ .700	+ .297	- .193	- .700	-1.078	-1.224	-1.205	-1.112	-1.066	-1.060	-1.074	-1.101	-1.118	-1.138	-1.153	-1.170	-1.172
3	6	1.295	+1	+ .947	+ .703	+ .286	- .214	- .692	-1.130	-1.269	-1.273	-1.186	-1.134	-1.122	-1.136	-1.164	-1.192	-1.218	-1.241	-1.261	-1.266
4.5	6	1.300	+1	+ .937	+ .706	+ .312	- .179	- .681	-1.116	-1.325	-1.297	-1.207	-1.139	-1.130	-1.149	-1.172	-1.203	-1.226	-1.241	-1.263	-1.275
6	6	1.316	+1	+ .936	+ .708	+ .320	- .162	- .685	-1.147	-1.390	-1.342	-1.229	-1.142	-1.148	-1.171	-1.176	-1.228	-1.251	-1.258	-1.265	-1.292
1.5	8	1.221	+1	+ .951	+ .710	+ .307	- .185	- .675	-1.065	-1.229	-1.196	-1.091	-1.042	-1.024	-1.044	-1.077	-1.103	-1.127	-1.145	-1.155	-1.157
3	8	1.279	+1	+ .946	+ .709	+ .297	- .194	- .699	-1.101	-1.274	-1.254	-1.167	-1.110	-1.098	-1.118	-1.146	-1.173	-1.194	-1.215	-1.234	-1.240
4.5	8	1.286	+ 1	+ .938	+ .704	+ .302	- .186	- .683	-1.102	-1.301	-1.282	-1.184	-1.120	-1.114	-1.129	-1.161	-1.183	-1.198	-1.218	-1.240	-1.252
6	8	1.285	+1	+ .933	+ .701	+ .304	- .186	- .679	-1.107	-1.335	-1.307	-1.182	-1.118	-1.122	-1.134	-1.170	-1.187	-1.198	-1.214	-1.240	-1.254
1.5	10	1.242	+1	+ .949	+ .716	+ .323	- .152	- .649	-1.030	-1.218	-1.198	-1.099	-1.054	-1.032	-1.052	-1.075	-1.099	-1.116	-1.131	-1.142	-1.148
3	10	1.279	+1	+ .942	+ .700	+ .296	- .200	- .697	-1.108	-1.281	-1.261	-1.170	-1.166	-1.102	-1.124	-1.150	-1.179	-1.197	-1.216	-1.236	-1.250
4.5	10	1.299	+1	+ .948	+ .711	+ .327	- .149	- .648	-1.064	-1.295	-1.283	-1.186	-1.155	-1.103	-1.123	-1.147	-1.174	-1.194	-1.210	-1.237	-1.245
6	10	1.300	+1	+ .950	+ .712	+ .333	- .139	- .642	-1.057	-1.304	-1.296	-1.190	-1.116	-1.105	-1.126	-1.149	-1.176	-1.201	-1.210	-1.239	-1.245

MODEL DIAMETER: 22.2 mm BLOCKAGE: 9%

R ÷ 10^4	A	C_d	C_p																	
			0^o	10^o	20^o	30^o	40^o	50^o	60^o	70^o	80^o	90^o	100^o	110^o	120^o	130^o	140^o	150^o	160^o	170^o	180^o
1.5	4	1.239	+1	+ .920	+ .653	+ .235	- .252	- .737	-1.134	-1.305	-1.209	-1.106	-1.089	-1.094	-1.115	-1.134	-1.158	-1.187	-1.219	-1.246	-1.255
3	4	1.304	+1	+ .922	+ .648	+ .226	- .273	- .784	-1.180	-1.362	-1.289	-1.163	-1.151	-1.163	-1.178	-1.215	-1.236	-1.271	-1.314	-1.341	-1.356
4.5	4	1.323	+1	+ .920	+ .662	+ .236	- .269	- .788	-1.200	-1.390	-1.304	-1.179	-1.163	-1.177	-1.198	-1.233	-1.265	-1.291	-1.333	-1.362	-1.384
6	4	1.346	+1	+ .929	+ .669	+ .239	- .264	- .793	-1.222	-1.427	-1.264	-1.185	-1.180	-1.204	-1.220	-1.251	-1.284	-1.320	-1.360	-1.385	-1.401
7.5	4	1.364	+1	+ .929	+ .669	+ .238	- .270	- .794	-1.230	-1.440	-1.248	-1.185	-1.193	-1.221	-1.233	-1.269	-1.297	-1.343	-1.380	-1.410	-1.418
9	4	1.374	+1	+ .931	+ .671	+ .242	- .272	- .787	-1.234	-1.449	-1.199	-1.173	-1.195	-1.225	-1.233	-1.275	-1.301	-1.358	-1.387	-1.423	-1.418
1.5	6	1.196	+1	+ .921	+ .658	+ .230	- .240	- .743	-1.117	-1.290	-1.172	-1.073	-1.060	-1.068	-1.078	-1.096	-1.123	-1.141	-1.166	-1.188	-1.202
3	6	1.280	+1	+ .923	+ .653	+ .231	- .272	- .801	-1.208	-1.388	-1.219	-1.134	-1.132	-1.143	-1.162	-1.194	-1.253	-1.252	-1.287	-1.310	-1.315
4.5	6	1.315	+1	+ .922	+ .661	+ .229	- .285	- .808	-1.226	-1.404	-1.218	-1.146	-1.147	-1.162	-1.188	-1.220	-1.250	-1.292	-1.318	-1.330	-1.342
6	6	1.329	+1	+ .924	+ .667	+ .238	- .277	- .785	-1.218	-1.415	-1.244	-1.157	-1.162	-1.189	-1.212	-1.238	-1.273	-1.312	-1.335	-1.361	-1.364
7.5	6	1.343	+1	+ .928	+ .669	+ .241	- .259	- .791	-1.225	-1.426	-1.247	-1.169	-1.180	-1.202	-1.221	-1.248	-1.285	-1.327	-1.351	-1.374	-1.379
9	6	1.350	+1	+ .932	+ .673	+ .245	- .229	- .798	-1.227	-1.435	-1.240	-1.176	-1.196	-1.204	-1.215	-1.250	-1.287	-1.334	-1.358	-1.374	-1.386

MODEL DIAMETER: 22.2 mm BLOCKAGE: 9%

R ÷ 10^4	A	C_d	C_p																	
			0^o	10^o	20^o	30^o	40^o	50^o	60^o	70^o	80^o	90^o	100^o	110^o	120^o	130^o	140^o	150^o	160^o	170^o	180^o
1.5	8	1.182	+1	+ .920	+ .665	+ .235	- .266	- .754	-1.135	-1.277	-1.167	-1.073	-1.047	-1.053	-1.074	-1.091	-1.100	-1.127	-1.144	-1.160	-1.186
3	8	1.260	+1	+ .926	+ .659	+ .229	- .327	- .781	-1.180	-1.354	-1.217	-1.118	-1.091	-1.221	-1.139	-1.176	-1.197	-1.241	-1.245	-1.265	-1.275
4.5	8	1.289	+1	+ .932	+ .670	+ .242	- .262	- .786	-1.192	-1.386	-1.201	-1.130	-1.124	-1.142	-1.171	-1.205	-1.227	-1.255	-1.282	-1.304	-1.313
6	8	1.310	+1	+ .928	+ .666	+ .236	- .276	- .788	-1.202	-1.390	-1.220	-1.147	-1.156	-1.172	-1.187	-1.229	-1.248	-1.280	-1.316	-1.335	-1.335
7.5	8	1.317	+1	+ .927	+ .663	+ .237	- .273	- .793	-1.217	-1,407	-1.224	-1.152	-1.168	-1.186	-1.199	-1.233	-1,257	-1.292	-1.327	-1.344	-1,348
9	8	1.316	+1	+ .925	+ .661	+ .242	- .266	- .799	-1.235	-1.432	-1.219	-1.152	-1.168	-1.191	-1.209	-1.224	-1.261	-1.297	-1.325	-1.348	-1.356
1.5	10	1.207	+1	+ .922	+ .655	+ .240	- .246	- .742	-1.094	-1.256	-1.195	-1.092	-1.051	-1.062	-1.076	-1.107	-1.122	-1.145	-1.177	-1.200	-1.207
3	10	1.247	+1	+ .920	+ .653	+ .240	- .258	- .754	-1.151	-1.312	-1.204	-1.095	-1.085	-1.108	-1.119	-1.146	-1.181	-1.208	-1.230	-1.251	-1.261
4.5	10	1.256	+1	+ .919	+ .649	+ .227	- .282	- .784	-1.179	-1.337	-1.237	-1.125	-1.108	-1.125	-1.148	-1.177	-1.204	-1.228	-1.252	-1.272	-1.285
6	10	1.274	+1	+ .919	+ .645	+ .214	- .290	- .802	-1.206	-1.365	-1.268	-1.147	-1.133	-1.149	-1.176	-1.201	-1.227	-1.259	-1.283	-1.306	-1.320
7.5	10	1.312	+1	+ .931	+ .672	+ .248	- .259	- .789	-1.223	-1.431	-1.222	-1.148	-1.155	-1.173	-1.189	-1.220	-1.249	-1.293	-1.319	-1.333	-1.336
9	10	1.309	+1	+ .927	+ .667	+ .253	- .265	- .816	-1.250	-1.462	-1.201	-1.148	-1.164	-1.181	-1.193	-1.218	-1.254	-1.303	-1.327	-1.339	-1.345

MODEL DIAMETER: 31.8 mm BLOCKAGE: 12.3%

R ÷ 10^4	A	C_d	C_p																	
			0°	10°	20°	30°	40°	50°	60°	70°	80°	90°	100°	110°	120°	130°	140°	150°	160°	170°	180°
1.5	4	1.306	+1	+ .926	+ .663	+ .254	- .263	- .762	-1.227	-1.432	-1.349	-1.197	-1.125	-1.164	-1.195	-1.206	-1.220	-1.264	-1.312	-1.355	-1.385
3	4	1.353	+1	+ .917	+ .645	+ .263	- .321	- .855	-1.283	-1.486	-1.339	-1.225	-1.224	-1.238	-1.254	-1.285	-1.319	-1.359	-1.400	-1.419	-1.443
4.5	4	1.374	+1	+ .916	+ .640	+ .202	- .327	- .865	-1.295	-1.498	-1.328	-1.256	-1.262	-1.269	-1.285	-1.316	-1.352	-1.392	-1.436	-1.472	-1.479
6	4	1.397	+1	+ .917	+ .641	+ .194	- .337	- .876	-1.313	-1.522	-1.349	-1.300	-1.287	-1.289	-1.316	-1.335	-1.377	-1.425	-1.468	-1.493	-1.505
7.5	4	1.418	+1	+ .915	+ .633	+ .182	- .333	- .872	-1.333	-1.542	-1.319	-1.270	-1.290	-1.318	-1.330	-1.373	-1.400	-1.450	-1.500	-1.517	-1.524
9	4	1.437	+1	+ .913	+ .631	+ .182	- .325	- .856	-1.332	-1.553	-1.309	-1.268	-1.313	-1.338	-1.349	-1.384	-1.424	-1.469	-1.513	-1.534	-1.542
10.5	4	1.429	+1	+ .912	+ .632	+ .180	- .347	- .900	-1.349	-1.549	-1.361	-1.300	-1.323	-1.338	-1.356	-1.387	-1.420	-1.462	-1.512	-1.546	-1.560
12	4	1.430	+1	+ .915	+ .637	+ .185	- .349	- .900	-1.340	-1.530	-1.395	-1.296	-1.315	-1.332	-1.350	-1.385	-1.415	-1.462	-1.505	-1.547	-1.555
1.5	6	1.263	+1	+ .925	+ .655	+ .221	- .271	- .794	-1.225	-1.433	-1.294	-1.189	-1.144	-1.150	-1.150	-1.180	-1.210	-1.250	-1.275	-1.290	-1.300
3	6	1.326	+1	+ .918	+ .642	+ .192	- .327	- .862	-1.309	-1.486	-1.336	-1.225	-1.212	-1.220	-1.242	-1.275	-1.315	-1.342	-1.379	-1.408	-1.417
4.5	6	1.343	+1	+ .915	+ .638	+ .189	- .337	- .875	-1.327	-1.493	-1.320	-1.229	-1.223	-1.240	-1.289	-1.300	-1.333	-1.364	-1.402	-1.431	-1.435
6	6	1.361	+1	+ .916	+ .636	+ .188	- .346	- .881	-1.328	-1.503	-1.314	-1.235	-1.243	-1.263	-1.294	-1.325	-1.358	-1.387	-1.427	-1.446	-1.450
7.5	6	1.380	+1	+ .920	+ .642	+ .192	- .342	- .882	-1.326	-1.523	-1.325	-1.252	-1.264	-1.284	-1.307	-1.338	-1.372	-1.407	-1.442	-1.469	-1.475
9	6	1.387	+1	+ .917	+ .640	+ .194	- .342	- .885	-1.330	-1.545	-1.337	-1.266	-1.276	-1.294	-1.316	-1.339	-1.381	-1.418	-1.452	-1.482	-1.492
10.5	6	1.387	+1	+ .913	+ .635	+ .195	- .344	- .889	-1.339	-1.568	-1.347	-1.278	-1.282	-1.299	-1.324	-1.334	-1.386	-1.425	-1.458	-1.490	-1.502
12	6	1.337	+1	+ .915	+ .637	+ .200	- .334	- .886	-1.342	-1.555	-1.354	-1.281	-1.252	-1.227	-1.245	-1.250	-1.325	-1.385	-1.435	-1.405	-1.436

MODEL DIAMETER: 31.8 mm BLOCKAGE: 12.3%

R ÷ 10^4	A	C_d	C_p																	
			0°	10°	20°	30°	40°	50°	60°	70°	80°	90°	100°	110°	120°	130°	140°	150°	160°	170°	180°
1.5	8	1.264	+1	+ .925	+ .685	+ .252	- .306	- .880	-1.263	-1.393	-1.336	-1.215	-1.180	-1.180	-1.190	-1.205	-1.255	-1.239	-1.267	-1.286	-1.317
3	8	1.318	+1	+ .916	+ .642	+ .208	- .313	- .837	-1.267	-1.459	-1.314	-1.195	-1.197	-1.202	-1.228	-1.259	-1.290	-1.328	-1.361	-1.377	-1.385
4.5	8	1.341	+1	+ .917	+ .641	+ .203	- .320	- .815	-1.276	-1.472	-1.301	-1.209	-1.214	-1.213	-1.246	-1.281	-1.318	-1.353	-1.385	-1.398	-1.426
6	8	1.356	+1	+ .919	+ .641	+ .200	- .330	- .850	-1.285	-1.476	-1.285	-1.217	-1.227	-1.249	-1.273	-1.302	-1.331	-1.367	-1.404	-1.428	-1.438
7.5	8	1.371	+1	+ .918	+ .638	+ .195	- .337	- .867	-1.305	-1.502	-1.301	-1.237	-1.248	-1.272	-1.291	-1.322	-1.354	-1.393	-1.425	-1.453	-1.465
9	8	1.386	+1	+ .917	+ .638	+ .190	- .343	- .880	-1.326	-1.532	-1.325	-1.261	-1.271	-1.293	-1.306	-1.341	-1.379	-1.420	-1.447	-1.476	-1.491
10.5	8	1.381	+1	+ .915	+ .648	+ .193	- .339	- .887	-1.331	-1.543	-1.331	-1.271	-1.292	-1.306	-1.311	-1.340	-1.377	-1.415	-1.441	-1.464	-1.475
12	8	1.376	+1	+ .913	+ .658	+ .195	- .336	- .895	-1.336	-1.555	-1.338	-1.280	-1.313	-1.319	-1.316	-1.338	-1.375	-1.411	-1.434	-1.451	-1.459

MODEL DIAMETER: 41.2 mm BLOCKAGE: 15.2%

R ÷ 10^4	A	C_d	C_p																	
			0°	10°	20°	30°	40°	50°	60°	70°	80°	90°	100°	110°	120°	130°	140°	150°	160°	170°	180°
1.5	4	1.345	+1	+ .947	+ .647	+ .221	- .338	- .853	-1.280	-1.471	-1.397	-1.279	-1.235	-1.176	-1.176	-1.250	-1.338	-1.353	-1.317	-1.441	-1.456
3	4	1.409	+1	+ .917	+ .624	+ .165	- .400	- .940	-1.400	-1.618	-1.515	-1.399	-1.335	-1.346	-1.371	-1.392	-1.430	-1.470	-1.510	-1.549	-1.559
4.5	4	1.414	+1	+ .913	+ .616	+ .159	- .393	- .933	-1.400	-1.635	-1.546	-1.400	-1.350	-1.357	-1.377	-1.400	-1.443	-1.471	-1.512	-1.560	-1.575
6	4	1.424	+1	+ .915	+ .621	+ .155	- .393	- .935	-1.408	-1.636	-1.555	-1.400	-1.350	-1.360	-1.380	-1.413	-1.452	-1.485	-1.525	-1.573	-1.595
7.5	4	1.436	+1	+ .913	+ .621	+ .150	- .390	- .930	-1.416	-1.645	-1.562	-1.408	-1.354	-1.366	-1.392	-1.418	-1.451	-1.495	-1.536	-1.580	-1.600
9	4	1.436	+1	+ .912	+ .618	+ .146	- .400	- .935	-1.432	-1.667	-1.583	-1.420	-1.371	-1.386	-1.406	-1.432	-1.463	-1.506	-1.548	-1.591	-1.610
10.5	4	1.445	+1	+ .913	+ .615	+ .144	- .416	- .945	-1.455	-1.696	-1.616	-1.436	-1.398	-1.409	-1.423	-1.451	-1.482	-1.519	-1.565	-1.606	-1.626
12	4	1.446	+1	+ .910	+ .613	+ .144	- .422	- .950	-1.470	-1.716	-1.643	-1.436	-1.415	-1.420	-1.430	-1.458	-1.488	-1.520	-1.570	-1.613	-1.634
15	4	1.445	+1	+ .908	+ .611	+ .137	- .430	- .994	-1.457	-1.548	-1.734	-1.504	-1.435	-1.427	-1.430	-1.449	-1.474	-1.519	-1.561	-1.609	-1.637
1.5	6	1.274	+1	+ .909	+ .644	+ .200	- .329	- .894	-1.316	-1.475	-1.355	-1.221	-1.187	-1.182	-1.204	-1.236	-1.262	-1.297	-1.330	-1.347	-1.376
3	6	1.347	+1	+ .913	+ .632	+ .177	- .350	- .900	-1.332	-1.544	-1.430	-1.312	-1.253	-1.260	-1.290	-1.322	-1.348	-1.389	-1.415	-1.450	-1.459
4.5	6	1.378	+1	+ .917	+ .629	+ .176	- .365	- .900	-1.355	-1.573	-1.465	-1.335	-1.290	-1.302	-1.323	-1.352	-1.379	-1.426	-1.455	-1.485	-1.504
6	6	1.381	+1	+ .915	+ .626	+ .158	- .376	- .934	-1.387	-1.593	-1.500	-1.346	-1.309	-1.322	-1.343	-1.376	-1.401	-1.438	-1.470	-1.500	-1.534
7.5	6	1.388	+1	+ .914	+ .629	+ .160	- .385	- .936	-1.391	-1.603	-1.504	-1.358	-1.323	-1.335	-1.350	-1.388	-1.411	-1.445	-1.474	-1.510	-1.529
9	6	1.389	+1	+ .912	+ .627	+ .161	- .390	- .942	-1.404	-1.621	-1.523	-1.361	-1.331	-1.343	-1.357	-1.391	-1.417	-1.451	-1.479	-1.517	-1.539
10.5	6	1.393	+1	+ .911	+ .626	+ .153	- .396	- .957	-1.427	-1.651	-1.564	-1.372	-1.352	-1.359	-1.373	-1.401	-1.432	-1.464	-1.497	-1.526	-1.546
12	6	1.394	+1	+ .910	+ .623	+ .155	- .405	- .969	-1.441	-1.671	-1.594	-1.386	-1.366	-1.368	-1.381	-1.408	-1.440	-1.471	-1.506	-1.531	-1.547
13.5	6	1.392	+1	+ .908	+ .620	+ .173	- .424	- .982	-1.445	-1.665	-1.600	-1.389	-1.378	-1.372	-1.378	-1.407	-1.437	-1.466	-1.505	-1.529	-1.551
15	6	1.398	+1	+ .912	+ .622	+ .160	- .394	- .964	-1.433	-1.679	-1.633	-1.405	-1.387	-1.381	-1.379	-1.410	-1.441	-1.467	-1.505	-1.533	-1.554

APPENDIX C - NOMENCLATURE

Symbol	Meaning
A	aspect ratio of cylinder, (L/D)
B	area blockage ratio
C_D	drag coefficient
C_p	pressure coefficient, $(p - p_o)/(\frac{1}{2} \rho U^2)$
C_{pb}	base-pressure coefficient measured at 180^o from stagnation point
D	cylinder diameter
f	frequency of vortex shedding
kU	local velocity at separation
m	wake area blockage ratio
p_o	tunnel static pressure
R	Reynolds number (UD/ν)
S	Strouhal number (fD/U)
x	distance along tunnel centre-line with the centre of cylinder as origin
y	distance normal to the plane of symmetry, with the centre of cylinder as origin
θ	angular distance around cylinder from stagnation point
ν	kinematic viscosity
ρ	density

APPENDIX D - REFERENCES

1. ALLEN, H.J., and VINCENTI, W.G. "Wall Interference in a Two-Dimensional wind tunnel, with Consideration of the Effect of Compressibility", N.A.C.A. Report No. 782, 1944.

2. FARELL, C., CARRASQUEL, S., GUVEN, O., and PATEL, O.C. "Effect of Wind-Tunnel Walls on the Flow Past Circular Cylinders and Cooling Tower Models", Trans. A.S.M.E.1., J. Fluids Engng, Vol. 99, 1977, pp 470-479.

3. GERRARD, J.H. "A Disturbance Sensitive Reynolds Number Range of the Flow Past a Circular Cylinder", J. Fluid Mech., Vol. No. 22, 1965, pp 187-196.

4. LIENHARD, J.H. "Synopsis of Lift, Drag, and Vortex Frequency Data for Rigid Circular Cylinders", Washington State Univ. Bull. No. 300, 1966.

5. MASKELL, E.C. "A Theory of the Blockage Effects of Bluff Bodies and Stalled Wings in a Closed Wind Tunnel", Aero Res. Counc. R. & M., No. 3400, 1963.

6. MODI, V.J., and EL-SHERBINY, S. "Effect on Wall Confinement on Aerodynamics of Stationary Circular Cylinders", Symp. on Wind Effects on Buildings and Structures, Tokyo, 1971.

7. MORKOVIN, M.V. "Flow Around a Circular Cylinder - a Kaleidoscope of Challenging Fluid Phenomena", A.S.M.E. Symp. on Fully Separated Flows, 1964, p 102.

8. PANKHURST, R.C., and HOLDER, D.W. Wind Tunnel Technique, 1952, Pitman.

9. ROSHKO, A., and FISZDON, W. "On the Persistence of Transition in the Near-Wake", Problems of Hydrodynamics and Continuum Mechanics, SIAM Philadelphia, 1969.

10. STANSBY, P.K. "The Effects of End Plates on the Base Pressure Coefficient of a Circular Cylinder", Aero. J., Vol. 78, 1974, pp 36-37.

11. WEST, G.S. "An Experimental Study of Blockage Effects on some Bluff Profiles", Dept of Civil Engng, Univ. of Qld Res. Rep. No.23, 1981.

CIVIL ENGINEERING RESEARCH REPORTS

CE No.	Title	Author(s)	Date
13	Combined Stiffness for Beam and Column Braces	O'CONNOR, C.	May, 1980
14	Beaches:- Profiles, Processes and Permeability	GOURLAY, M.R.	June, 1980
15	Buckling of Plates and Shells Using Sub-Space Iteration	MEEK, J.L. & TRANBERG, W.F.C.	July, 1980
16	The Solution of Forced Vibration Problems by the Finite Integral Method	SWANNELL, P.	August, 1980
17	Numerical Solution of a Special Seepage Infiltration Problem	ISAACS, L.T.	September, 1980
18	Shape Effects on Resistance to Flow in Smooth Semi-circular Channels	KAZEMIPOUR, A.K. & APELT, C.J.	November, 1980
19	The Design of Single Angle Struts	WOOLCOCK, S.T. & KITIPORNCHAI, S.	December, 1980
20	Consolidation of Axi-symmetric Bodies Subjected to Non Axi-symmetric Loading	CARTER, J.P. & BOOKER, J.R.	January, 1981
21	Truck Suspension Models	KUNJAMBOO, K.K. & O'CONNOR, C.	February, 1981
22	Elastic Consolidation Around a Deep Circular Tunnel	CARTER, J.P. & BOOKER, J.R.	March, 1981
23	An Experimental Study of Blockage Effects on Some Bluff Profiles	WEST, G.S.	April, 1981
24	Inelastic Beam Buckling Experiments	DUX, P.F. & KITIPORNCHAI, S.	May, 1981
25	Critical Assessment of the International Estimates for Relaxation Losses in Prestressing Strands	KORETSKY, A.V. & PRITCHARD, R.W.	June, 1981
26	Some Predications of the Non-homogenous Behaviour of Clay in the Triaxial Test	CARTER, J.P.	July, 1981
27	The Finite Integral Method in Dynamic Analysis : A Reappraisal	SWANNELL, P.	August, 1981
28	Effects of Laminar Boundary Layer on a Model Broad-Crested Weir	ISAACS, L.T.	September, 1981
29	Blockage and Aspect Ratio Effects on Flow Past a Circular Cylinder for $10^4 < R < 10^5$	WEST, G.S. & APELT, C.J.	October, 1981
30	Time Dependent Deformation in Prestressed Concrete Girder: Measurement and Prediction	SOKAL, Y.J. & TYRER, P.	November, 1981

CURRENT CIVIL ENGINEERING BULLETINS

4 *Brittle Fracture of Steel — Performance of ND1B and SAA A1 structural steels: C. O'Connor (1964)*

5 *Buckling in Steel Structures — 1. The use of a characteristic imperfect shape and its application to the buckling of an isolated column: C. O'Connor (1965)*

6 *Buckling in Steel Structures — 2. The use of a characteristic imperfect shape in the design of determinate plane trusses against buckling in their plane: C. O'Connor (1965)*

7 *Wave Generated Currents — Some observations made in fixed bed hydraulic models: M.R. Gourlay (1965)*

8 *Brittle Fracture of Steel — 2. Theoretical stress distributions in a partially yielded, non-uniform, polycrystalline material: C. O'Connor (1966)*

9 *Analysis by Computer — Programmes for frame and grid structures: J.L. Meek (1967)*

10 *Force Analysis of Fixed Support Rigid Frames: J.L. Meek and R. Owen (1968)*

11 *Analysis by Computer — Axisymetric solution of elasto-plastic problems by finite element methods: J.L. Meek and G. Carey (1969)*

12 *Ground Water Hydrology: J.R. Watkins (1969)*

13 *Land use prediction in transportation planning: S. Golding and K.B. Davidson (1969)*

14 *Finite Element Methods — Two dimensional seepage with a free surface: L.T. Isaacs (1971)*

15 *Transportation Gravity Models: A.T.C. Philbrick (1971)*

16 *Wave Climate at Moffat Beach: M.R. Gourlay (1973)*

17. *Quantitative Evaluation of Traffic Assignment Methods: C. Lucas and K.B. Davidson (1974)*

18 *Planning and Evaluation of a High Speed Brisbane-Gold Coast Rail Link: K.B. Davidson, et al. (1974)*

19 *Brisbane Airport Development Floodway Studies: C.J. Apelt (1977)*

20 *Numbers of Engineering Graduates in Queensland: C. O'Connor (1977)*